Deep CO_2 emitted at Furnas do Enxofre geothermal area (Terceira Island, Azores archipelago). An approach using carbon isotopic data

Fátima Viveiros[*1,2], Giovanni Chiodini[3], Carlo Cardellini[4], Stefano Caliro[5], Vittorio Zanon[1], Catarina Silva[1,6], Andrea Luca Rizzo[7], Ana Hipólito[1,8], Lucia Moreno[1,6]

1. *IVAR, Universidade dos Açores, Portugal*
2. *Faculdade de Ciências e Tecnologia, Universidade dos Açores, Portugal*
3. *INGV – Bologna (Italy)*
4. *Università degli Studi di Perugia, Dipartimento di Fisica e Geologia, Perugia (Italy)*
5. *INGV – Osservatorio Vesuviano*
6. *CIVISA, Portugal*
7. *INGV – Palermo (Italy)*
8. *IDL – Instituto Dom Luiz*

ABSTRACT

Quantification of the CO_2 released by the volcanoes to the atmosphere is relevant for the evaluation of the balance between deep-derived, biogenic and anthropogenic contributions. The current study estimates the CO_2 released from Furnas do Enxofre degassing area (Terceira Island, Azores archipelago) applying an approach that integrates the flux of CO_2 with its carbon isotopic compositions ($\delta^{13}C$), since the traditional geostatistical tools were not possible to apply due to the lack of spatial structure of the data. A deep-derived CO_2 output of 2.54 t d^{-1} is estimated for an area of ~ 23715 m^2. High biogenic-derived CO_2 flux values (~ 45 g m^{-2} d^{-1}) associated with light carbon isotopic content ($\delta^{13}C$ = -28‰ ± 1.1‰) are detected and explained by the vegetation that characterizes the study site. Carbon isotopic compositions of the CO_2 (-6.4‰ ± 1.2‰) measured in olivine-hosted fluid inclusions of the Terceira basalts are presented for the first time and contribute to define the mantle-CO_2 signature. Differences between these values and the heavier carbon imprints from the fumaroles existing in the Furnas do Enxofre degassing site (-4.66 ‰ to -4.27 ‰) are explained by the carbon isotopic fractionation occurring when CO_2 is precipitated as calcite in the geothermal reservoir with temperatures > 180ºC. A clear correlation between the soil temperature and deep CO_2 fluxes is observed and the integration of the diffuse degassing information with the composition of the fumarolic emissions allows estimating a thermal energy flux of 1.1 MW.

Highlights

- *Carbon isotopes of CO_2 effluxes differentiate deep vs shallow sources of CO_2;*
- *Carbon isotopes in fluid inclusions are relevant to define deep CO_2 signature;*
- *Fumarolic gas-geoindicators contribute to understand the degassing path;*
- *Vegetation data are crucial to characterize the biogenic CO_2 sources.*

Keywords: soil diffuse degassing, CO_2 fluxes, carbon isotopic composition, hydrothermal systems

1. Introduction

During the last decades several improvements have been made on the estimation of the amount of carbon dioxide emitted from volcanic soils to the atmosphere. These have been mainly related to the development of techniques and instruments that allowed an easy and quick measurement of soil CO_2 fluxes (e.g., Chiodini *et al*., 1998; Camarda *et al.*, 2006) and to improvements of probabilistic statistical tools used to perform degassing maps and estimate the CO_2 released to the atmosphere (Cardellini *et al*., 2003; Lewicki *et al*., 2005). Soil CO_2 degassing surveys have been carried out on various volcanic areas worldwide aiming, among others, at seismo-volcanic monitoring (*e.g*. Hernández *et al*., 2001; Inguaggiato *et al*., 2011; Werner *et al*., 2014; Liuzzo *et al*., 2015; Cardellini *et al*., 2017; Epiard *et al*., 2017; Bini *et al*., 2019), identification of hidden tectonic structures (Giammanco *et al*., 2006; Hutchison *et al*., 2015; Viveiros *et al*., 2017; Tamburello *et al*., 2018), definition of Carbon Capture and Storage or geothermal exploration areas (Schroder *et al*., 2016), and risk assessment (Viveiros *et al*., 2010; 2016; Barberi *et al*., 2019). Recent studies attempted to refine the CO_2 budget emitted from volcanic areas (Fisher *et al*., 2019; Werner *et al*., 2019) highlighting the relevant contribution of the diffuse degassing to the total flux of volcanic-hydrothermal CO_2 to the atmosphere.

Besides a mantle-derived origin, CO_2 emitted from soils in volcanic regions may have also a biogenic origin if measurements are performed in vegetated or organic matter-rich areas. Early studies discriminated possible CO_2 sources based on the CO_2 distribution of data on probability plots (Chiodini *et al*., 1998; Cardellini *et al*., 2003). Chiodini *et al*. (2008) set up a methodology that integrates soil CO_2 flux measurements and carbon isotopic composition of CO_2 efflux for the determination of the different gas sources. This method was first tested at the Solfatara (Phlegrean Fields, Italy) but proved to be a powerful tool to characterize the different sources feeding the CO_2

in various degassing areas (e.g., Viveiros *et al*., 2010; Parks *et al*., 2013; Lee *et al*., 2016; Hutchison *et al*., 2016).

Here we present the results of three soil CO_2 flux and temperature surveys undertaken at the hydrothermal site of Furnas do Enxofre (Terceira Island, Azores) between July 2013 and August 2014, along with carbon isotopic analyses of CO_2 collected during the last survey. Based on these data, this work estimates for the first time the soil CO_2 fluxes and the thermal energy released by the Furnas do Enxofre geothermal area, the only visible site of gas emissions at the Terceira volcanic Island. Since estimation of the hydrothermal CO_2 emitted from this degassing area was not possible using the commonly used geostatistical tools, due to the lack of spatial structure of the soil CO_2 flux datasets, a new methodology is here applied based on the measured carbon isotopic composition of the CO_2 efflux. A comprehensive discussion of the different sources contributing to the CO_2 outgassing is also done based on the type of vegetation found in the study area and the deep magmatic/hydrothermal carbon isotopic compositions measured both in olivine-hosted fluid inclusions and fumarolic emissions. We point out that the data of carbon isotopic composition of CO_2 in fluid inclusions of Terceira basalts are the first ever presented in Azores archipelago.

Gas composition of the hydrothermal fumaroles together with the deep-CO_2 estimations are finally used to calculate the thermal energy released from Furnas do Enxofre degassing area.

1.1 Geological and geothermal setting

The nine volcanic islands of the Azores archipelago (Portugal) are located in an area of lithospheric stretching, marking the triple junction of the Eurasian, American and Nubian tectonic plates (Searle, 1980). Several degassing manifestations as hydrothermal fumaroles, thermal and cold-CO_2 rich springs, and soil diffuse degassing areas characterize the volcanic activity in some of the islands (Ferreira *et al*., 2005; Caliro *et al*., 2015; Viveiros *et al*., 2017).

Terceira Island is located in the central part of the archipelago and comprises a fissure zone (that crosses the island along a general WNW-ESE direction) and four overlapping central volcanoes: Serra do Cume-Ribeirinha (also called Cinco Picos), Guilherme Moniz, Pico Alto and Santa Bárbara (Self, 1976) (Fig. 1). Central volcanoes are quiescent or extinct, while a subaerial (AD 1761) and two submarine eruptions (AD 1867 and AD 1998-2001) occurred from the fissure zone since the settlement of the islands in the 15th Century (Gaspar *et al.*, 2003; Pimentel *et al*., 2016).

The tectonic structures of Terceira mainly trend WNW-ESE to NW-SE (Madeira *et al*., 2015 and references therein). The latter fault system is well represented in the northeast sector of the island by the Lajes Graben (Fig. 1), where two major normal-dextral NWSE-oriented faults extend offshore for several kilometres (*e.g.*, Casalbore *et al*., 2015).

The only visible degassing area, known as Furnas do Enxofre, is located in the central part of the island at about 600 m altitude, on top of a trachytic lava dome partly superimposed by a lava *coulée*, at the southeast flank of Pico Alto Volcano (Ferreira *et al.*, 2005). This volcano is older than 141 ka and it is covered by numerous lava domes and *coulée* (Gertisser *et al*., 2010). Two main zones with visible fumarolic emissions are identified at Furnas do Enxofre and only recently the chemical and isotopic composition of CO_2 of the fumarolic fluids was determined (Caliro *et al*., 2015). The fumaroles show a typical hydrothermal composition with water vapour as the main component of the fluids emitted (>96 vol.%), followed by CO_2 and H_2S. Based on Chiodini and Marini (1998) geothermometers, an equilibrium temperature of approximately 190 ºC was inferred for the hydrothermal system feeding the fumaroles (Caliro *et al*., 2015).

Carbon isotopic composition of the CO_2 released by the fumaroles, expressed as δ‰ vs. V-PDB, ranges between -4.66 ‰ and -4.48 ‰ (Caliro *et al*., 2015). The helium isotopic composition shows a value of approximately 9.6 Ra (being Ra the $^3He/^4He$ of atmospheric helium equal to $1.39 \cdot 10^{-6}$; Ozima and Podosek, 2002), which overlaps the range of values measured on Terceira rock samples by Moreira *et al*. (1999) and Madureira *et al.* (2005) (9.7±1.1 Ra), but is significantly lower than the two values estimated by Jean-Baptiste *et al.* (2009) (12.8 and 13.5 Ra). Recent CO_2 flux measurements carried out in Algar do Carvão volcanic lake, about 1.4 km east from Furnas do Enxofre degassing area, showed very low CO_2 emissions of biogenic origin (Andrade *et al*., 2019). Furnas do Enxofre is also classified as one of the 38 geothermal wetlands of international importance since 2008 by the Ramsar Convention (list available in http://www.ramsar.org/), and the mean annual precipitation in the area varies between 1000 and 2000 mm (Bettencourt, 1979).

A pilot binary geothermal power plant of about 3.5 MW, ~ 1 km far from Furnas do Enxofre fumaroles, in the so-called Pico Alto Geothermal Field (Franco *et al*., 2017) started operating in November 2017 (Fig. 1). The high temperature geothermal reservoir is liquid-dominated and maximum temperatures >300ºC have been measured in the drilled wells, being the roof of the reservoir located at about 500-600 m (Franco *et al*., 2017; Thorsteinsdóttir, 2017).

2. Sample and analytical methodologies

2.1 Soil diffuse degassing

Three soil CO_2 flux surveys were carried out at Furnas do Enxofre fumarolic field (July/August 2013; May 2014 and August 2014). The area is characterised by clayey soils (dominated by kaolinite) and irregular topography with a central hollowed area. Dispersed steaming fractured zones are visible around the depressed area. A total of 932 measurements were performed with the accumulation chamber method (Chiodini *et al*., 1998), using a portable fluxmeter manufactured by the West Systems S.r.l. The instrument is equipped with a LICOR LI-800 infrared (L-IR) CO_2 detector (analytical range 0 - 2 vol.%), which was calibrated before each of the field surveys. A reproducibility of about 10% was calculated by Chiodini *et al*. (1998) for this technique, and Carapezza and Granieri (2004) refined this estimation up to 24% for low soil CO_2 flux values. Simultaneous soil temperature measurements, at 20 cm depth, were carried out with a portable thermocouple (thermometer Testo 925 with resolution of 0.1 ºC in the -50 to 200 ºC range).

In the first two surveys the sampled sites were distributed as homogeneously as possible considering the irregular topography. During August 2014 survey, an approximate square regular grid of 10 m space, was adopted; this survey was performed by two teams, and the calibration of the two used instruments was checked by comparison of several measurements in the same sites; gas samples for the determination of the carbon isotope composition of the CO_2 efflux were also collected in 99 of the 281 sampled sites following the methodology described by Chiodini *et al*. (2008). In detail, a t-connector valve is inserted in the flow line between the accumulation chamber and the CO_2 detector and ~15 ml of sample is extracted and inserted in a 12 ml evacuated vial. Two samples at different CO_2 concentrations were collected for each site. Samples were analysed within few days at the Laboratory of Fluid Geochemistry of the Istituto Nazionale di Geofisica e Vulcanologia-Osservatorio Vesuviano (INGV-OV). CO_2 concentrations (C_{CO2}) and carbon isotopic compositions ($\delta^{13}C_{CO2}$) were determined by coupling a gas chromatograph (Agilent Technologies 6890N) with a continuous flow mass spectrometer (Finnigan Delta plus XP). The CO_2 concentration standard error is ±5% and for the $\delta^{13}C$ is ±0.2‰) (for more details see Chiodini *et al*., 2008). The carbon isotopic composition of the CO_2 efflux was computed using the following mass balance equation (Chiodini *et al*., 2008):

$$\delta^{13}C_{efflux} = \frac{\delta^{13}C_{CO2,B} \times C_{CO2,B} - \delta^{13}C_{CO2,A} \times C_{CO2,A}}{C_{CO2,B} - C_{CO2,A}} \qquad (1)$$

Where the letters A and B refer, respectively, to the first and second gas sample collected at each site.

Soil CO_2 fluxes from the three surveys, temperatures, A and B concentrations-isotopic compositions of data acquired in August 2014 are reported in the Supplementary material (Table A.1).

Considering the significant influence that environmental variables may have on the soil gas flux (*e.g*., Oliveira *et al*., 2018), data recorded by the permanent GTER1 station, located at Furnas do

Enxofre area since December 2002 (Ferreira *et al*., 2005), were used as control point to check the intra and inter-survey variability of the soil CO_2 flux.

2.2 Fumarolic emissions

Fumarolic gases were collected at Furnas do Enxofre on the 26th August 2014 in 200 ml pre-evacuated flasks containing approximately 50 ml 4N NaOH solution (Giggenbach, 1975; Giggenbach and Goguel, 1989). Incondensable gases were also collected in 20 ml glass bottles equipped with two stopcocks by passing the fumarolic gases through a water-cooled condenser. The chemical and isotopic analyses of the gas emissions were carried out at the Laboratory of Fluids Geochemistry of the Istituto Nazionale di Geofisica e Vulcanologia – Osservatorio Vesuviano (INGV-OV) using a Finnigan Delta plusXP continuous flow mass spectrometer coupled with an Agilent Technologies 6890 gas chromatograph. Additional details about the analytical procedures are found on Caliro *et al.* (2015).

The isotopic composition of He ($^3He/^4He$) and ^{20}Ne was determined at the Noble Gas Isotope Laboratory of the INGV - Sezione di Palermo (INGV-Palermo). Gases where introduced into an ultra-high-vacuum (10^{-9}–10^{-10} mbar) purification line, in which all of the species in the gas mixture, except noble gases, were removed under getters. Prior to the analysis, He and Ne were separated from Ar by adsorbing the latter in a charcoal trap cooled by liquid nitrogen (77 K). He and Ne were then adsorbed in a cryogenic trap connected to a cold head cooled with a He compressor to ≤10 K. Helium was desorbed at 42 K and admitted into a GVI-Helix SFT mass spectrometer. After restoring the ultra-high vacuum in the cryogenic trap, Ne was released at 82 K and then admitted into a Thermo-Helix MC Plus mass spectrometer. The analytical uncertainty of He-isotope ratio measurements (1σ) was <1%, while that of ^{20}Ne was <0.1%. The same procedure was adopted for the He and Ne isotope measurements of the air standards (*e.g.*, Rizzo *et al*., 2016, 2019), whose reproducibility conditions are comparable to those reported for fluid inclusions (see Section 4.1). Typical blanks for He and Ne were $<10^{-15}$ and $<10^{-16}$ mol, respectively, being at least two orders of magnitude lower than samples signals at the mass spectrometer. Helium isotope ratios are reported in the form of R_C/R_A, where R_C is the air-corrected $^3He/^4He$ ratio of the sample, assessed based on $^4He/^{20}Ne$ ratios:

$R_C/R_A = [(R_M/R_A)(He/Ne)_M - (He/Ne)_{air}]/[(He/Ne)_M - (He/Ne)_{air}]$, where subscripts "M" and "air" refer, respectively, to measured and atmospheric theoretical values. Further details on the analytical protocol can be found in Rizzo *et al.* (2016, 2019).

2.3 Gases trapped in fluid inclusions

Carbon, helium ($^3He/^4He$) and ^{20}Ne isotopic compositions were measured in fluid inclusions hosted in olivine assemblages of three basaltic rocks erupted from the fissure zone (Fig. 1). Preparation of the minerals and analyses of the fluid composition were done at the Noble Gas Isotope laboratory of INGV-Palermo, following a defined protocol (*e.g.*, Rizzo *et al.*, 2015; 2018), in which un-weathered crystals have been checked for the presence of volcanic glass attached to the crystals rim and then cleaned in an ultrasonic bath with successive treatments in diluted acid (6.5% HNO_3), deionized water, and ultra-pure acetone for 15 minutes. Distinct aliquots of each sample (0.4 - 1.9 g) have been handpicked under a microscope. The selected crystals were split into two aliquots: the first was loaded into a stainless-steel crusher capable of holding up to six samples simultaneously for noble-gas extraction and analysis, while the second was used for determining the concentration and isotope ratio of CO_2. Noble gases trapped inside fluid inclusions were released by in-vacuum single-step crushing at ~200 bars. This procedure is the most conservative to minimize the contribution of cosmogenic ^3He and radiogenic ^4He possibly grown/trapped in the crystal lattice (*e.g.*, Kurz, 1986; Hilton *et al.*, 1993, 2002). The CO_2 concentration measurement was first performed during noble gas extraction at the time of crushing by quantifying the total gas pressure (CO_2+N_2+O_2+noble gases) and subtracting the residual pressure of N_2+O_2+noble gases after removing CO_2 using a "cold finger" immersed in liquid N_2 at −196 ºC. The noble gases were then cleaned in an ultra-high-vacuum (10^{-9}–10^{-10} mbar) purification line, and all species in the gas mixture, except for noble gases, were removed. He isotopes (^3He and ^4He) and ^{20}Ne were measured separately using two different split-flight-tube mass spectrometers (Helix SFT, Thermo Scientific). The analytical uncertainty of the He-isotope ratio (1σ) was <1%, while this was <0.1% for ^{20}Ne. The reported values of ^{20}Ne are corrected for isobaric interference at m/z values of 20 ($^{40}Ar^{2+}$). Typical blanks for He, Ne, and Ar were $<10^{-15}$, $<10^{-16}$, and $<10^{-14}$ mol, respectively, with negligible influence on samples signals at the mass spectrometer. Further details about the analytical procedures are available in Rizzo *et al*. (2018). The CO_2 samples used in the analyses of C isotopes were extracted and quantified in a glass line, which avoids the adsorption and fractionation of CO_2 that can occur in powders and upon contact with stainless steel. After purification, CO_2 was trapped in a glass sampler and moved to the INGV-Palermo stable-isotope laboratory for the isotope measurements. Further details about the extraction and analytical protocol can be found in Gennaro *et al.* (2017). The $^{13}C/^{12}C$ is expressed in delta notation ($\delta^{13}C$) as the difference in parts per mil relative to the V-PDB international standard. The analytical error estimated as 1σ was better than 0.3‰.

3. Results and discussion

3.1 Fumarolic gas composition

The two main fumaroles located at Furnas do Enxofre were sampled in August 2014, concurrently with the soil CO_2 flux survey. Outlet maximum temperatures of 97.2 ºC were measured and data collected in 2013, which were already published in a paper focused on the gas manifestation of the entire Azores archipelago (Caliro *et al.*, 2015), are also used to complement the studies of the fumarolic gas composition (Tables 1 and 2).

The five gas samples show a clear hydrothermal composition with water vapour as the main component followed by CO_2 (2.6%-3.7% by volume), H_2 (0.022%-.035%) and H_2S (0.021%-0.032%), and minor contents of the other gas species. Methane concentrations are also quite high (118-185 ppm), comparing to the other Azorean fumarolic fields (Caliro *et al*., 2015).

C-O-H *gas equilibria*

Gas equilibria within the H_2O-H_2-CO_2-CH_4-CO gas system are here considered to investigate T-P-redox conditions of the system feeding the fumaroles. In detail, the method of Chiodini and Marini (1998) was adopted and it assumes an equilibrium condition among all the species of the system. For fumarolic fluids deriving from a boiling hydrothermal system, the method allows the estimation of the temperature, the fluid pressures, the redox conditions, and the phase feeding the fumarolic effluents (*e.g*., equilibrated vapour phase, liquid phase, vapour separated by the boiling of a liquid, etc.). Contemporarily, a specie by specie check of equilibrium is done to assess the reliability of the estimations.

In detail, the formation reactions of the various species are combined in order to eliminate the f_{O2} variable and to estimate the equilibrium temperature in suitable diagrams of the obtained combined functions (*e.g*., the diagram 3 $\log(X_{CO}/X_{CO2}) + \log(X_{CO}/X_{CH4})$ vs $\log(X_{H2O}/X_{H2}) + \log(X_{CO}/X_{CO2})$, see Chiodini and Marini 1998 for further details). The Terceira fumaroles plot close to the line representing the saturated vapour phase at temperatures of 186-212°C (Fig. 2).

A specie by specie check confirms the reliability of such temperature estimations: the X_{H2}/X_{H2O}, X_{CO}/X_{CO2} and X_{CH4}/X_{CO2} log ratios plot in fact close to the equilibrated vapour phase for a redox buffer (*i.e*., that of D'Amore and Panichi, 1980), typical of many worldwide hydrothermal systems (Chiodini and Marini, 1998), when plotted against the equilibrium temperatures estimated in figure 2 (Fig. 3).

Beside the temperatures, we computed also the H_2O and CO_2 fugacities (f_{H2O} and f_{CO2} from equations 1 and 55 in Chiodini and Marini, 1998) that allow us to investigate the conditions controlling the CO_2 fugacity in the system feeding the Furnas do Enxofre fumaroles. In the stability diagram of figure 4, the estimated f_{CO2} and temperatures are compared with the theoretical values expected for hydrothermal and metamorphic reactions involving CO_2. The Furnas do Enxofre fumaroles plot close to the so called "full equilibrium" line (Giggenbach, 1988) suggesting that the f_{CO2} is fixed, in a full equilibrium hydrothermal system, by univariate reactions involving calcite, a Ca-Al-silicate, K-feldspar, K-mica and chalcedony (Giggenbach, 1984, 1988).

The C-O-H equilibrium temperatures and pressure (P_{tot} in bar assumed equal to $f_{H2O} + f_{CO2}$) are finally compared with the temperature profiles of the Pico Alto geothermal wells (Fig. 5, Franco *et al.,* 2017). The gas equilibration zone, whose depth of 130-200 m is computed from P_{tot} assuming a hydrostatic control, is located close to the change in the slope of the thermal gradients of the wells (Fig. 5). This picture is consistent with the presence of a gas zone, at 190-210°C, located at the top of a geothermal system characterised at depth by higher temperatures (up to 300°C, Fig. 5).

Origin of the gas species

The origin of the gas species of Furnas do Enxofre fumaroles are highly discussed in Caliro *et al.* (2015) in the frame of a general work regarding the gas emission of the entire Azores archipelago. The data collected in 2014 (integrated with those published by Caliro *et al*., 2015; Table 2) confirm previous interpretations: (i) the fumarolic H_2O is of meteoric origin; (ii) the un-reactive gas species He, Ar and N_2, derive from the mixing between an atmospheric component, mainly air dissolved in groundwater, and a deep magmatic component; (iii) the high $^3He/^4He$ isotopic ratios (Rc/Ra of ~ 9.6, practically the same in the five different samples) suggest that magmatic fluids with a plume-like (lower mantle) contribution feeds this hydrothermal system. It is worth noting that similar high $^3He/^4He$ ratios (from 9.19 to 9.62 Ra) were measured in CO_2-rich fluid inclusions hosted in olivine crystals handpicked from basalts erupted in the island (Table 2). According to Zanon and Pimentel (2015), the analyzed CO_2-rich fluid inclusions are trapped at the Moho Transition Zone (20.3 to 21 km depth) below the Terceira fissure zone (Fig.1), and a second step of fluid entrapment below the central zone of Terceira Island is located at a depth between 16.5 and 8.5 km. These fluid inclusions have a carbon isotopic composition of CO_2 ($\delta^{13}C$) ranging from -6.12‰ to -5.95‰, which is slightly lighter than that measured in the fumaroles ($\delta^{13}C$ from -4.66‰ to -4.27‰). This difference however is not large and can be explained by the carbon isotopic fractionation occurring when the CO_2 is precipitated as calcite in the geothermal reservoir. This fractionation at temperatures > 180°C forms calcite with a carbon isotopic composition lighter than the parental CO_2 (Friedman and O'Neil, 1977). Practically, the relatively light mantle CO_2 entering the deepest and hottest zones of the hydrothermal system will become heavier in the fumaroles since part of the CO_2 is precipitated as hydrothermal calcite at temperatures > 180°C, what is in agreement with the temperatures measured in the reservoir (Fig. 5; Franco *et al*., 2017).

3.2 Soil diffuse degassing

Three soil diffuse degassing surveys were carried out at Furnas do Enxofre fumarolic area and descriptive statistics of the several measured variables are displayed in table 3. In what concerns the permanent soil CO_2 flux station (GTER1), only data recorded during the surveyed period (daytime, during the spatial measurements) are displayed. The data recorded by the permanent station during the surveys are available as supplementary material (Table A.2).

Soil CO_2 fluxes span in large intervals in the three surveys, generally from few g m^{-2} d^{-1} to thousands of g m^{-2} d^{-1}, indicating the presence of multiple CO_2 sources (biogenic and volcanic-hydrothermal) and/or the occurrence of other factors such as, for example, soils with different permeability and distinct transferring mechanisms of the gases trough the soils (advective or diffusive processes). The probability plots of log soil CO_2 fluxes of the three surveys well describe this complexity since the points distribute in curves characterised by the presence of two inflection points for all the surveys (Fig. 6). This distribution of the flux is consistent with the overlapping of three log-normal populations (A-low, B-intermediate and C-high CO_2 flux populations, Fig. 6). Based on the method of Sinclair (1974) and Chiodini *et al*. (1998), we estimate for each survey the mean (μ), standard deviations (σ) and fractions (f) of the log normal populations. Since the computed statistical parameters refer to the logarithm of CO_2 flux values, the mean value of CO_2 flux and the central 90% confidence interval of the mean are estimated by means of the Sichel's t estimator (David, 1977) (Table 4).

Permanent GTER1 station recorded soil CO_2 flux values between 86 and 267 g m^{-2} d^{-1} during the surveyed periods (Table 3). The intra-survey coefficient of variation varied between 12 and 17%, respectively, for S1 and S2. These variations are considered acceptable when compared with the reproducibility of the CO_2 flux measurements, which was estimated as varying between 10% and 24% (Chiodini *et al*., 1998; Carapezza and Granieri, 2004). The coefficient of variation estimated considering the three surveys increased to 25%, showing a significantly higher inter-survey variation that can easily be explained by seasonal effects (e.g., Viveiros *et al.*, 2014).

3.2.1 CO_2 sources feeding the diffuse emission

High CO_2 flux populations (populations referenced as C in table 4, with mean values higher than 364 g m^{-2} d^{-1}) are representative of the almost pure deep-derived CO_2, while the other populations (A and B) could represent either the biogenic or the deep source, or a mixture between them. In order to better determine and characterise the sources of the CO_2, numerous measurements of the carbon isotopic composition of the CO_2 efflux ($\delta^{13}C_{efflux}$, see equation 1) were performed in August

2014. As mentioned by Chiodini *et al*. (2008), this method allows to differentiate the deep *vs*. biogenic contribution for each measured flux.

The computed $\delta^{13}C_{efflux}$ varies between -30.4‰ and -4.1‰ (Table A.1) and the probability plot of the values (Fig. 7) shows the overlapping of the following three populations: population *bio* ($\delta^{13}C_{bio}$ = -28‰ ± 1.1‰; $f = 0.46$), population *mix* ($\delta^{13}C_{mix}$ = -18‰ ± 7‰; $f = 0.22$) and population *deep* ($\delta^{13}C_{deep}$ = -6.4‰ ± 1.2‰; $f = 0.32$). Note that the estimated isotopic composition of populations *bio* and *deep* are well compatible with biogenic and deep CO_2 sources, while the intermediate population *mix* refers to the mixtures between the two pure end-members.

Once defined the isotopic composition of the deep and of the biogenic CO_2, we computed, sample by sample, the specific fluxes of the two end-members (*deep*CO_2 and *bio*CO_2 fluxes in the following). Soil CO_2 fluxes with $\delta^{13}C_{efflux}$ below -28‰ + 1.1‰ (mean population *bio* + 1σ, 40 samples) were considered pure *bio*CO_2 fluxes, whereas fluxes with $\delta^{13}C_{efflux}$ above -6.4‰ ± 1.2‰ (mean population *deep* - 1σ, 27 samples) were considered pure *deep*CO_2 fluxes. For the remaining 32 intermediate samples the relative contribution of biogenic and deep end-members are computed according to the following set of equations:

$$\delta^{13}C_{efflux} = X\ \delta^{13}C_{deep} + (1 - X)\ \delta^{13}C_{bio} \qquad (2)$$

From equation 2, the fraction (X) of the deep CO_2 is given by the following equation:

$$X = \frac{\delta^{13}C_{efflux} - \delta^{13}C_{bio}}{\delta^{13}C_{deep} - \delta^{13}C_{bio}} \qquad (3)$$

The *deep*CO_2 flux is then calculated as the fraction X of the measured CO_2 flux:

$$deepCO_2\,flux = X \times measuredCO_2\,flux \qquad (4)$$

while the *bio*CO_2 flux is computed as the difference between the measured CO_2 flux and the *deep*CO_2 flux. The pure *bio*CO_2 and *deep*CO_2 fluxes are plotted in the log probability diagram of Fig. 7b for quantifying the mean fluxes generated by the two sources. It follows a brief discussion about the two sources.

Biogenic CO_2

The *bio*CO_2 flux at Furnas do Enxofre degassing area has a mean of 44.8 ± 3.8 g $m^{-2}d^{-1}$ (Fig. 7b), which is relatively high with respect to what generally found in numerous hydrothermal sites around the world (Chiodini *et al*., 2008 and references therein). This value is significantly higher even comparing to other degassing areas of the archipelago, such as Furnas Volcano located at São Miguel Island, where a value of 25 g m^{-2} d^{-1} was estimated as the biogenic threshold (Viveiros *et al*., 2010). Vegetation coverage found out specifically in the Furnas do Enxofre area may contribute to explain these high values: bryophytes (essentially *Sphagnum spp*.) cover most of the exposed cliffs, and the vascular vegetation observed around the main degassing area is dominated by *Calluna vulgaris* with some endemic plants (*Vaccinium cylindraceum*) (Costa, 2011 and references therein). A study carried out with bryophytes in a temperate rainforest (DeLucia *et al*., 2003) shows that net carbon uptake by these mosses is small, and corresponds to a small fraction (only about 10%) of the CO_2 released by soils respiration, consequently releasing most of the CO_2 to the atmosphere. This, together with the fact that the total respiration from the forest floor, including CO_2 efflux from bryophytes roots and soil microbial activity, increases with soil water content and soil temperature, may justify the high biogenic CO_2 fluxes found out at Furnas do Enxofre degassing site. In fact, these conditions are reached in the study area with average soil temperature between 29 and 33ºC, and high water content as testified by Bettencourt (1979) as well as its classification as Ramsar site.

From the $\delta^{13}C_{efflux}$ values (Fig. 7a) we estimated a $\delta^{13}C$ of -28‰, for the pure *Biogenic* CO_2, a value slightly lower of what has been found in other areas (*e.g*., -19.4 ‰ at Solfatara, -25‰ at Santorini, < -25‰ in Ethiopia, Chiodini *et al*., 2008; Parks *et al*., 2013; Hutchison *et al*., 2016). This lighter value is, however, consistent with the type of vegetation of the area. Furnas do Enxofre is in fact dominated by the presence of C3 plants (bryophytes and the vascular *Calluna vulgaris*) that exhibit lighter carbon isotope compositions (-20 to -37‰) when compared with C4 plants. Farquhar *et al*., (1989) and Kohn (2010) estimated a global average composition of -28.5‰ for the $\delta^{13}C$ values of C3 plants, considering also the inverse correlation observed between $\delta^{13}C$ and precipitation, which is significantly high in the study area as mentioned above. In addition, Huang *et al*. (1997) measured carbon isotopic compositions of – 28‰ to -27‰ for the *Calluna vulgaris*, one of the dominant vascular plants at Furnas do Enxofre (Costa, 2011 and references therein). The vegetation found out in the study area is therefore in agreement both with the relatively light isotopic composition of the carbon and the relatively high biogenic CO_2 fluxes measured, highlighting the importance of characterizing the vegetation existing in hydrothermal areas.

Deeply derived CO_2

The isotopically derived mean *deep*CO_2 flux of 483 ± 134 g $m^{-2}d^{-1}$ (Fig. 7b) is close to the mean of Population C3, estimated only based on the statistical distribution of the flux data (466 g $m^{-2}d^{-1}$, Fig. 6 and Table 4). The source of this CO_2 should be quite deep, as suggested by its isotopic signature ($\delta^{13}C_{deep}$ = -6.4‰ ± 1.2‰), which is similar to the isotopic composition of the CO_2 trapped on the fluid inclusions of Terceira basaltic rocks (-6.03‰) and captured at the Moho Transition Zone depths (as high as ~21 km, Zanon and Pimentel, 2015). The heavier isotopic signature measured in the fumaroles (-4.5‰, Table 2) is probably explained by the precipitation of calcite in the hydrothermal system.

3.2.2 Mapping of CO_2 flux and estimation of the total deep CO_2 output

Mapping soil CO_2 degassing is a valuable tool to visualize the spatial distribution of the soil degassing allowing to identify anomalous CO_2 areas, define the extension and the shape of the diffuse degassing structures (DDS) (Chiodini *et al*., 2001), and estimate the amount of CO_2 emitted to the atmosphere (*i.e*., the CO_2 output). Cardellini *et al*. (2003) used for the first time a geostatistical approach, based on sequential Gaussian simulations (sGs), to perform soil CO_2 flux mapping, to compute the CO_2 output and the associated uncertainty (see methods). To reliably apply this geostatistical method, the data have to follow a normal distribution and have to be spatially correlated (*i.e*., the experimental variogram needs to show spatial structure; Deutsch and Journel, 1998; Cardellini *et al*., 2003). The experimental variograms of the CO_2 flux from the first two surveys (Supplementary material A.3) instead showed a lack of spatial correlation (*i.e*. pure nugget effect). Taking into consideration these results, the survey carried out on August 2014 was planned based on a roughly regular grid, to investigate if the absence of correlation was due to the sampling strategy. August 2014 measurements were performed along well-established profiles in the field and measurements were taken each 10 m, as much as the topography allowed. Nevertheless, also the variogram of the August 2014 CO_2 fluxes does not show any clear spatial structure.

For this reason, the total CO_2 output from the deep source was estimated using the graphical statistical analysis methodology (GSA) described by Chiodini *et al*. (1998) that consists in multiplying the mean flux of the high flux populations (Table 4) by the fraction of the population and the extension of the surveyed areas. This method indicates total deep CO_2 output from 1.91 t d^{-1} to 6.18 t d^{-1} for the three surveys (Table 4). In order to compare the different results, the deep CO_2 output is recalculated as a standardised value per area, since the extension of the surveyed area is not the same for the three campaigns. Standardised values range in a narrower interval (76.4-

112.8 t d^{-1} km^{-2}) with the minimum value estimated for May 2014 and the maximum for the 2013 survey (Table 4). When these values are compared with the average soil CO_2 fluxes recorded by GTER1 station during the surveys (Table 3), a positive correlation (R^2 ~ 0.93) is observed suggesting the adequacy of the permanent station to represent the flux released in the entire degassing area.

An alternative approach to map and to estimate the deep CO_2 output with sGs was attempted by using as input data only the *deep*CO_2 flux computed as described in section 4.2.1. For this attempt we used the 99 samples of August 2014 for which the isotopic composition of the CO_2 efflux is available. This dataset was subdivided in two subsets according to their location (Fig. 8). Contrary to the total datasets, the variograms of the *deep*CO_2 flux show a good spatial structure allowing both to map the deep CO_2 emission and to estimate the corresponding deep CO_2 output. Interestingly, the same model fits the variograms of the subset areas (Fig. 8a). As a general consideration, this result indicates how the biogenic CO_2 produced in the soil can hide the deep signal by introducing a random type variability.

The total deep CO_2 output results in 2.54 t d^{-1}, *i.e.*, slightly higher than the emission computed by the GSA approach for the same survey (2.21 t d^{-1}, Table 4). The difference could be due to the intermediate population B3 that partly includes a deep CO_2 contribution and that is not considered in the GSA approach. Our conclusion is that the 2.54 t d^{-1} is the most reliable estimate because the evident biases possibly affecting the GSA estimations of the total deep CO_2 output, especially in this area characterised by relatively high fluxes from the biogenic source and not so high deep CO_2 fluxes.

3.3 Soil temperature anomalies and thermal energy release

Soil temperature varied between 17.3 and 99.8 ºC in the surveyed area (Table 3). Contrarily to the soil CO_2 flux datasets, experimental variograms for the soil temperature show a well-defined spatial structure and, consequently, soil temperature maps were performed for the three surveys by applying sequential Gaussian simulations (Fig. 8b and 9).

Soil temperature anomalous zones with temperature > 90 ºC occur in the NW side of the sampled area close to the fumarolic vents; a second anomalous area, in the SE sector, is highlighted in the survey performed in August 2014 (Fig. 8b) and marginally in the 2013 survey, since this is an area quite difficult to access due to the topography and type of vegetation. High soil CO_2 flux values are in general associated to the highest temperatures, however the presence of low soil CO_2 fluxes measured close to the anomalous zones, as well as possibly high soil CO_2 fluxes from the biogenic source in areas far from the thermal anomalies, explain the significant spatial heterogeneity in the soil CO_2 flux compared to the soil temperature.

When the deep CO_2 flux derived by the isotopic measurements is considered, such different behaviour of soil temperature and flux disappears, resulting in a strict similitude between the deep CO_2 flux and soil temperature maps (Fig. 8). This correspondence is well explained by the upraise of hydrothermal vapours that approaching the surface locally condense generating anomalous flux of heat (temperature anomaly) and of incondensable gases (deep CO_2 anomaly). This is the optimal situation for the estimation of the thermal energy release associated to the degassing process (Chiodini *et al*., 2005), a computation that, for the above reasons, is restricted to the survey of August 2014. The thermal energy released by the shallow condensation of the steam (QH_{cond}, in kJ/s) is given by the total flux of steam that condenses (Q_{cond}, in kg/s) multiplied by the difference between the enthalpy of the steam at the condensation temperature of 100°C ($H_{V,100}$ in kJ/kg) and the enthalpy of the liquid at ambient temperature ($H_{L,20}$ in kJ/kg):

$$QH_{cond} = Q_{cond} \times (H_{V,100} - H_{L,20}) \qquad (5)$$

where Q_{cond} can be computed by multiplying the total deep CO_2 emission (Q_{CO2}, expressed in kg/s) by the H_2O/CO_2 ($R_{H2O/CO2}$) fumarolic weight ratio assumed as representative of the pre-condensed vapours ($Q_{cond} = Q_{CO2} \times R_{H2O/CO2}$). From equation 5 the thermal energy released by the condensation of the steam originally associated with the deep CO_2 results as 1132 kJ/s (1.13 MW) (Table 5).

4. Conclusions

Three surveys have been carried out at Furnas do Enxofre degassing site aiming to estimate the deep-derived CO_2 flux emissions from the area. However, the lack of clear spatial continuity of the soil CO_2 flux data did not allow to perform reliable soil CO_2 flux maps through the widely used sGs approach (Cardellini *et al*., 2003). The graphical statistical procedure (Chiodini *et al*., 1998) was thus used to estimate the total CO_2 output, which varied between 1.91 t d^{-1} and 6.18 t d^{-1}, for the surveys carried out, respectively, in May 2014 and in the Summer 2013. These differences are also explained by the different extent of the surveyed areas, and standardized fluxes per area varied between 76.4 and 112.8 t d^{-1} km^{-2} (Table 4). During August 2014 a more regular survey was defined and 281 measurements were performed using a rough 10 m grid. Samples for carbon isotopic detection were also collected in 99 sites following the methodology described by Chiodini *et al*. (2008), but absence of spatial structure was still observed for the CO_2 fluxes. The lack of spatial continuity is probably explained by the high biogenic CO_2 contribution in combination with relatively low deep-derived CO_2 fluxes. In one hand, the high biogenic CO_2 fluxes are caused by the local vegetation, mainly bryophytes that may release high CO_2 (DeLucia *et al*., 2003), together with the wet and warm conditions of the soils; in the other hand, the deep CO_2 is emitted preferentially from hydrothermally altered clayey soils located close to the fumaroles, which may hamper the gas release at the surface and, probably, may favour its accumulation in sub-superficial layers. The carbon isotopic composition of the CO_2 efflux allowed us to quantitatively separate each single measurement in biogenic and deep CO_2 flux (*bio*CO_2 and *deep*CO_2 flux). It is worth noting that the recalculated *deep*CO_2 fluxes, contrary to the measured ones, show a spatial structure and allow both mapping and estimating a total deep CO_2 emission (2.54 t d^{-1}). The good correlation between the maps of *deep*CO_2 fluxes and the soil temperatures points to the upflow of vapours from the hydrothermal system that, approaching the surface, locally condense generating anomalous flux of heat and incondensable gases. The thermal energy associated to the process is estimated as 1.13 MW.

The method based on the carbon isotopic composition of the CO_2 efflux, allowed us to determine also the carbon isotopic signature of the pure deep and biogenic CO_2. The significantly light carbon isotopic compositions ($\delta^{13}C$ of -28‰) determined for the pure biogenic CO_2 is consistent with the C3 plants, which are the dominant vegetation type in the area. The deep CO_2 isotopic signature determined in the CO_2 efflux ($\delta^{13}C_{deep}$ = -6.4‰) is similar to both CO_2 trapped in fluid inclusions from basalts from Terceira Island ($\delta^{13}C$ ~ -6 ‰), which are formed at depths down to 21 km, and the CO_2 emitted by the fumaroles ($\delta^{13}C$ ~ -4.5‰) that are formed from the boiling of a local hydrothermal system.

Gases collected from these fumaroles have been used to estimate the gas equilibrium conditions. The H_2O-H_2-CO_2-CH_4-CO gas system (Chiodini and Marini, 1998) results at equilibrium at temperatures of 186 to 212 ºC (Fig. 2) in a saturated vapour phase. These inferred conditions are consistent with the data available from the close Pico Alto geothermal wells (Fig. 5; Franco *et al*., 2017).

As general consideration, future eventual compositional variations of the fumarolic emissions may be relevant to detect changes correlated with either the geothermal exploitation or the volcanic activity. In this frame, it is worth to mention that historical accounts report visual changes in the degassing regime of Furnas do Enxofre fumaroles in the months preceding the 1761 volcanic eruption (Pimentel *et al*., 2016). In the current period of volcanic quiescence, our study shows stability on the gas compositions (Table 1) between the surveys carried out in 2013 (Caliro *et al*., 2015) and 2014. Another important tool to continuously monitor the hydrothermal degassing in relation to volcanic activity and geothermal exploitation is the CO_2 flux automatic station (GTER1) that was installed at Pico Alto in 2002 (Ferreira *et al*., 2005). The CO_2 flux continuously measured by GTER1 shows a good agreement with the CO_2 emission estimated in the different surveys (Tables 3 and 4).

Ultimately, this study highlights the importance of specific isotopic measurements of the CO_2 efflux in order to obtain reliable estimations of the gas flux and for the definition of the isotopic imprint of the pure carbon sources active in an area. Furthermore, the application of the current methodology in other degassing areas of the Earth will allow more reliable estimations of the total volcanic CO_2 budgets.

Acknowledgements

This study was partially funded by the DECADE initiative from the Deep Carbon Observatory through the grant "TERCO$_2$ – Soil CO_2 released at Terceira volcanic island". Preparation of the document was also carried out on the scope of the project Heatstore-Geothermica Era-net and MIUR project n. PRIN2017-2017LMNLAW "Connect4Carbon". We thank Mariagrazia Misseri, and Mariano Tantillo for helping in noble gas measurements and CO_2 extraction from minerals, as well as Fausto Grassa and Ygor Oliveri for the carbon isotopic measurements of CO_2 from fluid inclusions at INGV-Palermo.

REFERENCES

Andrade C., Viveiros F., Cruz J.V., Coutinho R., Branco R., (2019). CO_2 fluxes of two lakes in volcanic caves in the Azores, Portugal. *App. Geochem*., 102:218-228.

Barberi F., Carapezza M.L., Tarchini L., Ranaldi M., Ricci T., Gattuso A. (2019). Anomalous Discharge of Endogenous Gas at Lavinio (Rome, Italy) and the Lethal Accident of 5 September 2011. *Geohealth*, 3:407-422. https://doi.org/10.1029/2019GH000211.

Bettencourt M.L. (1979). *O clima dos Açores como recurso natural na aplicação especialmente em agricultura e indústria do turismo*, Lisboa, Instituto Nacional de Meteorologia e Geofísica (in Portuguese).

Bini G., Chiodini G., Cardellini C., Vougioukalakis G.E., Bachmann O. (2019). Diffuse emission of CO_2 and convective heat release at Nisyros caldera (Greece). *J. Volcanol. Geotherm. Res*., 376:44-53.

Caliro S., Viveiros F., Chiodini G., Ferreira T. (2015). Gas geochemistry of hydrothermal fluids of the S. Miguel and Terceira Islands, Azores. *Geochim. Cosmochim. Acta*, 168:43-57. doi:10.1016/j.gca.2015.07.009.

Camarda M., Gurrieri S., Valenza M. (2006). CO_2 flux measurements in volcanic areas using the dynamic concentration method: influence of soil permeability. *J. Geophys. Res*., 111, B05202. doi:10.1029/2005JB003898.

Carapezza M.L., Granieri D. (2004). CO_2 soil flux at Vulcano (Italy): comparison between active and passive methods. *Appl. Geochem*., 19:73-88.

Cardellini C., Chiodini G., Frondini F. (2003). Application of stochastic simulation to CO_2 flux from soil: Mapping and quantification of gas release. *J. Geophys. Res*. 108, 2425. doi: 10.1029/2002JB002165.

Cardellini C., Chiodini G., Frondini F., Avino R., Bagnato E., Caliro S., Lelli M., Rosiello A. (2017). Monitoring diffuse volcanic degassing during volcanic unrests: The case of Campi Flegrei (Italy). *Sci. Rep*., 7, 6757. doi: 10.1038/s41598-017-06941-2.

Casalbore D., Romagnoli C., Pimentel A., Quartau R., Casas D., Ercilla G., Hipólito A., Sposato A., Chiocci F.L. (2015). Volcanic, tectonic and mass-wasting processes offshore Terceira Island (Azores) revealed by high-resolution seafloor mapping. *Bull. Volcanol*., 77:24.

Chiodini G., Caliro S., Cardellini C., Avino R., Granieri D., Schmidt A. (2008). Carbon isotopic composition of soil CO_2 efflux, a powerful method to discriminate different sources feeding soil CO_2 degassing in volcanic-hydrothermal areas. *Earth Planet. Sci. Lett*., 274:372–379.

Chiodini G., Cioni R., Guidi M., Raco B., Marini L. (1998). Soil CO_2 flux measurements in volcanic and geothermal areas. *Appl. Geochem*., 13:543–552.

Chiodini G., Frondini F., Cardellini C., Granieri D., Marini L., Ventura G. (2001). CO_2 degassing and energy release at Solfatara Volcano, Campi Flegrei, Italy. *J. Geophys. Res*., 106:16213-16221.

Chiodini G., Granieri D., Avino R., Caliro S., Costa A., Werner C. (2005). Carbon dioxide diffuse degassing and estimation of heat release from volcanic and hydrothermal systems, *J. Geophys. Res.*, 110, B08204, doi:10.1029/2004JB003542.

Chiodini G., Marini L. (1998). Hydrothermal gas equilibria: The H_2O-H_2-CO_2-CO-CH_4 system. *Geochim. Cosmochim. Acta,* 62:2673-2687.

Costa M.R. (2011). *Contributo para o estudo do campo geotermal das Furnas do Enxofre (Ilha Terceira) e implicações no Plano de Gestão*. Master thesis (in Portuguese), University of the Azores, 156p.

David M. (1977). *Geostatistical Ore Reserve Estimation*. Elsevier Scientific Publishing Company, Amsterdam, 364pp.

D'Amore F., Panichi C. (1980). Evaluation of deep temperatures of hydrothermal systems by a new gas geothermometer. *Geochim. Cosmochim. Acta,* 44:549-556.

DeLucia E., Turnbull M.H., Walcroft A.S., Griffins K.L., Tissue D.T., Glenny D., Mcseveny T.M., Whitehead, D. (2003). The contribution of bryophytes to the carbon exchange for a temperate rainforest. *Global Change Biol*., 9:1158-1170.

Deutsch C.V., Journel, A.G. (1998). *GSLIB: Geostatistical Software Library and User's Guide*. Applied Geostatistics Series. Oxford Univerity Press, New York Oxford, 369p.

Epiard M., Avard G., Maarten de Moor J., Cruz M.M., Castillo G.B., Bakkar H. (2017). Relationship between Diffuse CO_2 Degassing and Volcanic Activity. Case Study of the Poás, Irazú, and Turrialba Volcanoes, Costa Rica. *Front. Earth Sci*., 5:71. doi: 10.3389/feart.2017.00071.

Farquhar G.D., Ehleringer J.R., Hubick K.T. (1989). Carbon isotope discrimination and photosynthesis. *Annu. Rev. Plant Physiol. Plant Mol. Biol*., 40:503-537.

Ferreira T., Gaspar J.L., Viveiros F., Marcos M., Faria C., Sousa F. (2005). Monitoring of fumarole discharge and CO_2 soil degassing in the Azores: contribution to volcanic surveillance and public health risk assessment. *Ann. Geophys*., Vol. 48, N. 4/5:787-796.

Fischer T.P., Arellano S., Carn S., Aiuppa A., Galle B., Allard P., Lopez T., Shinohara H., Kelly P., Werner C., Cardellini C., Chiodini G. (2019). The emissions of CO_2 and other volatiles from the world's subaerial volcanoes. *Sci. Rep*., 9:18716. https://doi.org/10.1038/s41598-019-54682-1.

Franco A., Vieira N., Ponte C. (2017). Geothermal development in Pico Alto, Terceira Island, Portugal. *GRC Transactions*, 41.

Friedman I., O'Neil J.R. (1977). Compilation of stable isotope fractionation factors of geochemical interest: *U.S. Geological Survey Professional Paper 440*, 11 p.

Gaspar J.L., Queiroz G., Pacheco J.M., Ferreira T., Wallenstein N., Almeida M.H., Coutinho R. (2003). Basaltic lava balloons produced during the 1998–2001 Serreta submarine ridge eruption (Azores). In: White J.D.L., Smellie J.L., Clague D.A. (Eds.) *Explosive subaqueous volcanism*. AGU Geophysical Monograph 140, pp.205–212.

Gennaro M.E., Grassa F., Martelli M., Renzulli A., Rizzo A.L. (2017). Carbon isotope composition of CO_2-rich inclusions in cumulate-forming mantle minerals from Stromboli volcano (Italy). *J. Volcanol. Geotherm. Res*., 346:95-103. DOI:10.1016/j.jvolgeores.2017.04.001

Gertisser R., Self S., Gaspar J.L., Kelley S.P., Pimentel A., Eikenberg J., Barry T.L., Pacheco J.M., Queiroz G., Vespa M. (2010). Ignimbrite stratigraphy and chronology on Terceira Island, Azores. In: Groppelli G., Viereck-Goette L. (Eds.) *Stratigraphy and geology of volcanic areas*. GSA Special Paper 464, pp.133–154.

Giammanco S., Gurrieri S., Valenza M. (2006). Fault-controlled soil CO_2 degassing and shallow magma bodies: summit and lower east rift of Kilauea volcano (Hawaii), 1997. *Pure Appl. Geophys*., 163:853-867.

Giggenbach W.F. (1975). A simple method for the collection and analysis of volcanic gas samples. *Bull.Volcanol*. 39:132-145.

Giggenbach W.F. (1984). Mass transfer in hydrothermal alteration systems - a conceptual approach. *Geochim. Cosmochim. Acta*, 48:2693-2711.

Giggenbach W.F. (1987). Redox processes governing the chemistry of fumarolic gas discharges from White Island, New Zealand. *Appl. Geochem*., 2:143-161.

Giggenbach W.F. (1988). Geothermal solute equilibria. Derivation of Na-K-Mg-Ca geoindicators. *Geochim. Cosmochim. Acta*, 52:2749.

Giggenbach W.F., Goguel R.L. (1989). Collection and analysis of geothermal volcanic water and gas discharges. Chemistry Division, DSIR, *New Zealand. Report no. CD 2401*.

Hernández P.A., Notsu K., Salazar J.M., Mori T., Natale G., Okada H., Virgili G., Shimoike Y., Sato M., Pérez N.M. (2001) - Carbon dioxide degassing by advective flow from Usu Volcano, Japan. *Science*, 292: 83-86.

Hilton D.R., Fisher T.P., Marty B. (2002). Noble gases and volatile recycling at subduction zones. *Rev. Mineral. Geochem*. 47:319–370. doi: 10.2138/rmg.2002.47.9.

Hilton D.R., Hammerschmidt K., Loock G., Friedrichsen H. (1983). Helium and argon isotope systematics of the central Lau Basin and Valu Fa Ridge: Evidence of crust/mantle interactions in a back-arc basin. *Geochim. Cosmochim. Acta,* 57(12):2819-2841.

Huang Y., Eglington G., Ineson P., Latter P.M., Bol R., Harkness D.D. (1997). Absence of carbon isotope fractionation of individual n-alkanes in a 23-year field decomposition experiment with Calluna vulgaris. *Organic Geochem*., 26:497-401. 10.1016/S0146-6380(97)00027-2.

Hutchison W., Biggs J., Mather T.A., Pyle D.M., Lewi E., Yirgu G., Caliro S., Chiodini G., Clor L.E., Fischer T.P. (2016). Causes of unrest at silicic calderas in the East African Rift: New constraints from InSAR and soil-gas chemistry at Aluto volcano, Ethiopia. *Geochem. Geophys. Geosyst*., 17: 3008–3030. doi:10.1002/2016GC006395.

Hutchison W., Mather T.A., Pyle D.M., Biggs J., Yirgu G. (2015). Structural controls on fluid pathways in an active rift system: A case study of the Aluto volcanic complex. *Geosphere*, 11(3): 542-562.

Inguaggiato S., Vita F., Rouwet D., Bobrowski N., Morici S., Sollami A. (2011). Geochemical evidence of the renewal of volcanic activity inferred from CO_2 soil and SO_2 plume fluxes: the 2007 Stromboli eruption (Italy). *Bull. Volcanol*., 73:443-456.

Jean-Baptiste P., Allard P., Coutinho R., Ferreira T., Fourré E., Queiroz G., Gaspar J.L. (2009). Helium isotopes in hydrothermal volcanic fluids of the Azores archipelago. *Earth Planet. Sci. Lett.*, 281:70-80.

Keenan J.H., Keyes F.G., Hill P.G., Moore J.G. (1969). *Steam Tables: Thermodynamic Properties of Water Including Vapor, Liquid, and Solid Phases*, John Wiley, Hoboken, N. J., 162 pp.

Kohn M.J. (2010). Carbon isotope compositions of terrestrial C3 plants ad indicators of (paleo)ecology and (paleo)climate. *PNAS*, 107(46):19691.

Kurz M. (1986). Cosmogenic helium in a terrestrial igneous rock. *Nature.* 320:435-439.

Lee H., Muirhead J.D., Fischer T.P., Ebinger C.J., Kattenhorn S.A., Sharp Z.D., Kianji G. (2016). Massive and prolonged deep carbon emissions associated with continental rifting. *Nature Geosci*., 5p. doi:10.1038/NGEO2622.

Lewicki J.L, Bergfeld D., Cardellini C., Chiodini G., Granieri D., Varley N., Werner C. (2005). Comparative soil CO_2 flux measurements and geostatistical estimation methods on Masaya volcano, Nicaragua. *Bull. Volcanol*., 68:75-90.

Liuzzo M., Di Muro A., Giudice G., Michon L., Ferrazzini V., Gurrieri S. (2015). New evidence of CO_2 soil degassing anomalies on Piton de la Fournaise volcano and the link with volcano tectonic structures. *Geochem. Geophys. Geosyst*., 16. doi:10.1002/2015GC006032.

Madeira J., Brum da Silveira A., Hipólito A., Carmo R. (2015). Active tectonics in the Central and Eastern Azores islands along the Eurasia-Nubia boundary: a review. In Gaspar J.L., Guest J.E., Duncan A.M., Barriga F.J.A.S., Chester D.K. (Eds.) *Volcanic Geology of S. Miguel Island (Azores archipelago).* Geological Society, London, Memoirs. 44:15-32.

Madureira P., Moreira M., Mata J., Allègre C.J. (2005). Primitive neon isotopes in Terceira Island (Azores archipelago). *Earth Planet. Sci. Lett.* 233:429-440.

Moreira M., Doucelance R., Kurz M.D., Dupré B., Allègre C.J. (1999). Helium and lead isotope geochemistry of the Azores Archipelago. *Earth Planet. Sci. Lett*. 169:189-205.

Ozima M., Podosek F.A. (2002). *Noble gas geochemistry*. Cambridge University Press, UK.

Parks M.M., Caliro S., Chiodini G., Pyle D.M., Mather T.A., Berlo K., Edmonds M., Biggs J., Nomikou P., Raptakis C. (2013). Distinguishing contributions to diffuse CO_2 emissions in volcanic areas from magmatic degassing and thermal decarbonation using soil gas $^{222}Rn–\delta^{13}C$ systematics: Application to Santorini volcano, Greece. *Earth Planet. Sci. Lett*., 377-378:180-190.

Pimentel A., Zanon V., De Groot L.V., Hipólito A., Di Chiara A., Self S. (2016). Stress-induced comenditic trachyte effusion triggered by trachybasalt intrusion: multidisciplinary study of the AD 1761 eruption at Terceira Island (Azores). *Bull. Volcanol*., 78(3):22. doi:10.1007/s00445-016-1015-6.

Quartau R., Hipólito A., Romagnoli C., Casalbore D., Madeira J., Tempera F., Roque C., Chiocci F. L. (2014). The morphology of insular shelves as a key for understanding the geological evolution of volcanic islands: Insights from Terceira Island (Azores). *Geochem. Geophys. Geosyst.,* 15:1801-1826. doi:10.1002/2014G005248.

Rizzo A.L., Barberi F., Carapezza M.L., Di Piazza A., Francalanci L., Sortino F., D'Alessandro W. (2015). New mafic magma refilling a quiescent volcano: evidence from He-Ne-Ar isotopes during the 2011–2012 unrest at Santorini, Greece. *Geochem. Geophys. Geosyst*., 16:798–814. doi: 10.1002/2014GC005653.

Rizzo A.L., Caracausi A., Chavagnac V., Nomikou P., Polymenakou P., Mandalakis M., Kotoulas G., Magoulas A., Castillo A., Lampridou D. (2016). Kolumbo submarine volcano (Greece): An active window into the Aegean subduction system. *Sci. Rep*., 6:28013. doi: 10.1038/srep28013.

Rizzo A.L., Caracausi A., Chavagnac V., Nomikou P., Polymenakou P.N., Mandalakis M., Kotoulas G., Magoulas A., Castillo A., Lampridou D., Marusczak N. Sonke J.E. (2019). Geochemistry of CO_2-Rich Gases Venting from Submarine Volcanism: The Case of Kolumbo (Hellenic Volcanic Arc, Greece). *Front. Earth Sci*., 7:60. doi: 10.3389/feart.2019.00060.

Rizzo A.L., Pelorosso B., Coltorti M., Ntaflos T., Bonadiman C., Matusiak-Małek M., Italiano F., Bergonzoni G. (2018). Geochemistry of Noble Gases and CO_2 in Fluid Inclusions from Lithospheric Mantle Beneath Wilcza Góra (Lower Silesia, Southwest Poland). *Front. Earth Sci*., 6:215. doi: 10.3389/feart.2018.00215.

Searle R. (1980). Tectonic pattern of the Azores spreading centre and triple junction. *Earth Planet. Sci. Lett*., 51:415-434.

Self S. (1976). The recent volcanology of Terceira, Azores. *J. Geol. Soc. Lond*., 132:645–666.

Tamburello G., Pondrelli S., Chiodini G., Rouwet D. (2018). Global-scale control of extensional tectonics on CO_2 earth degassing. *Nat. Commun*., 9:4608. https://doi.org/10.1038/s41467-018-07087-z.

Thorsteinsdóttir, U. (2017). *A 3D geological static field model of the Krafla geothermal area, NE-Iceland; constructing a workflow applied to the Pico Alto geothermal area, Azores*, Master Thesis, Faculty of Earth Sciences, University of Iceland, 143pp.

Viveiros F., Cardellini C., Ferreira T., Caliro S., Chiodini G., Silva C. (2010). Soil CO_2 emissions at Furnas volcano, Sao Miguel Island, Azores archipelago: volcano monitoring perspectives, geomorphologic studies, and land use planning application. *J. Geophys. Res*., 115: B12208. doi:10.1029/2010JB007555.

Viveiros F., Gaspar J.L., Ferreira T., Silva C. (2016). Hazardous indoor CO_2 concentrations in volcanic environments. *Environ. Pollut*., 214: 776-786, doi:10.1016/j.envpol.2016.04.086.

Viveiros F., Marcos M., Faria C., Gaspar J.L., Ferreira T., Silva C. (2017). Soil CO_2 Degassing Path along Volcano-Tectonic Structures in the Pico-Faial-São Jorge Islands (Azores Archipelago, Portugal). *Front. Earth Sci*., 5:50. doi:10.3389/feart.2017.00050.

Viveiros F., Vandemeulebrouck J., Rinaldi A.P., Ferreira T., Silva C., Cruz J.V. (2014). Periodic behavior of soil CO_2 emissions in diffuse degassing areas of the Azores archipelago: Application to seismovolcanic monitoring. *J. Geophys. Res*., 119(10):7578-7597. doi: 10.1002/2014JB011118.

Werner C., Bergfeld D., Farrar C.D., Doukas M.P., Kelly P.J., Kern C. (2014). Decadal-scale variability of diffuse CO_2 emissions and seismicity revealed from long-term monitoring (1995-2013) at Mammoth Mountain, California, USA. *J. Volcanol. Geotherm. Res*., 289:51-63.

Werner C., Fischer T., Aiuppa A., Edmonds M., Cardellini C., Carn S., Chiodini G., Cottrell E., Burton M., Shinohara H., Allard P. (2019). Carbon dioxide emissions from subaerial volcanic regions. *Two decades in review. Deep Carbon: Past to Present*. Cambridge University Press.

Captions

Figure 1. Location of the study area: Terceira Island volcanic systems and the main tectonic structures (modified from Quartau *et al*., 2014) with the location of the Furnas do Enxofre study site. Blue squares represent the location of the basaltic samples used for fluid inclusions analyses. Terceira Island is highlighted as red square in the Azores archipelago inset at the top right of the figure.

Figure 2. Gas ratio diagram of log 3 (X_{CO}/X_{CO2}) + log ($_{XCO}/X_{CH4}$) vs log (X_{H2O}/X_{H2}) + log (X_{CO}/X_{CO2}). The theoretical values of both variables in a single saturated vapour phase, in a single saturated liquid phase, in the vapours produced during a single step boiling of an original liquid at temperature T_0 and of the vapours separated at different separation temperatures Ts are shown. In the left of the diagram is reported the field of superheated vapours or steam condensation (see Chiodini and Marini, 1998 for further details). The theoretical compositions are compared with the analytical gas ratios of the Terceira fumaroles.

Figure 3. Diagram of log X_{CH4}/X_{CO2}, log X_{CO}/X_{CO2}, and log X_{H2}/X_{H2O} vs. 1000/T(K). Theoretical ratios in a single saturated vapour phase, under redox conditions controlled by the hydrothermal f_{O2} buffers (FeO)-($FeO_{1.5}$) of Giggenbach (1987) and D'Amore and Panichi (1980) are shown for reference. Theoretical ratios expected for a vapour in equilibrium with a brine and redox conditions fixed by the magmatic SO_2-H_2S buffer (Giggenbach, 1987) are also plotted. Analytical ratios for the fumaroles of Furnas do Enxofre (grey circles) are plotted against the equilibrium temperatures calculated through H_2-CO_2-CO-CH_4-H_2O equilibria.

Figure 4. Plot of f_{CO2} vs equilibrium temperatures calculated for the equilibrium single saturated vapour phase feeding Furnas do Enxofre fumaroles (grey circles). The full equilibrium function of Giggenbach (1988) and f_{CO2}, T values of relevant metamorphic reactions are also shown for comparison (redraw from Chiodini and Marini, 1998).

Figure 5 Elevation and temperature of the gas equilibration zone of Furnas do Enxofre fumaroles compared with the stabilized temperature profiles of the Pico Alto geothermal wells (grey lines, data from Franco *et al*., 2017). The wells are about 1 km distant from the fumaroles. The elevation of the gas equilibration zone is estimated considering a depth of 120-200 m (P_{tot} from 12 to 20 bar) from the water table, assumed at 500 m of elevation.

Figure 6. Log probability plot of the soil CO_2 fluxes measured during the three surveys. Populations identified as "A", "B" and "C" refer, sequentially to the biogenic, intermediate and deep-derived CO_2 sources.

Figure 7. (a) Probability plot of the $\delta^{13}C_{efflux}$ (b) Log probability plot of the CO_2 flux from the pure biogenic and deep sources (*bio*CO_2 flux and *deep*CO_2 flux, respectively).

Figure 8. a) Deep soil CO_2 flux and b) soil temperature interpolated map for Furnas do Enxofre fumarolic area based on the data collected on August 2014. The experimental variograms are inserted in the figures with the black and white circles representing, respectively, variograms of the west and east areas. Both maps were modelled with spherical variograms using the following parameters: CO_2 fluxes - nugget = 0.43; sill = 1.12; range = 60; soil temperature NW area (black line): nugget = 0.22; sill = 1.21; range = 72; soil temperature SE area (grey line): nugget = 0.22; sill = 1.15; range = 40. Red circles represent Furnas do Enxofre fumaroles; empty dots represent all the sampled sites and the black dots the carbon isotopes measurement sites.

Figure 9. Soil temperature interpolated maps for the two surveys performed at Furnas do Enxofre fumaroles in Summer 2013 (a) and May 2014 (b). Sampled points are displayed as black points in the maps. The experimental variograms are inserted in the figures. Both maps were modelled with spherical variograms using the following parameters: Summer 2013 map - nugget = 0.14; sill = 1.12; range = 95; May 2014: nugget = 0.06; sill = 1.28; range = 110.

Table 1. Chemical compositions (expressed in mmol/mol) of the Furnas do Enxofre fumaroles. Samples from October 2013 respect to the study carried out by Caliro *et al.* (2015). The coordinates refer to the WGS84 UTM 26S.

Table 2. Isotopic compositions of the Furnas do Enxofre fumaroles and fluid inclusions found out in olivines of basalts. Isotopic compositions of N, C, O and H are expressed, respectively, in delta notation per mil vs. Atmosphere, V-PDB and V-SMOW. The He isotopic compositions are expressed as Rc/Ra. * refers to the samples from Caliro *et al*. (2015); *n.d*. – not detected.

Table 3. Descriptive statistics of the variables sampled at Furnas do Enxofre diffuse degassing area during the surveys. S1, S2 and S3 identify, respectively, first, second and third surveys.

Table 4. Estimated statistical parameters from the partitioned CO_2 flux populations and 90% confidence interval of the mean based on the Sichel's t estimator (David, 1977). Total CO_2 output estimated based on the graphical statistical analysis methodology (GSA).

Table 5. Thermal energy released by the condensation of hydrothermal steam at Furnas do Enxofre study site (enthalpy values from Keenan *et al*., 1969).

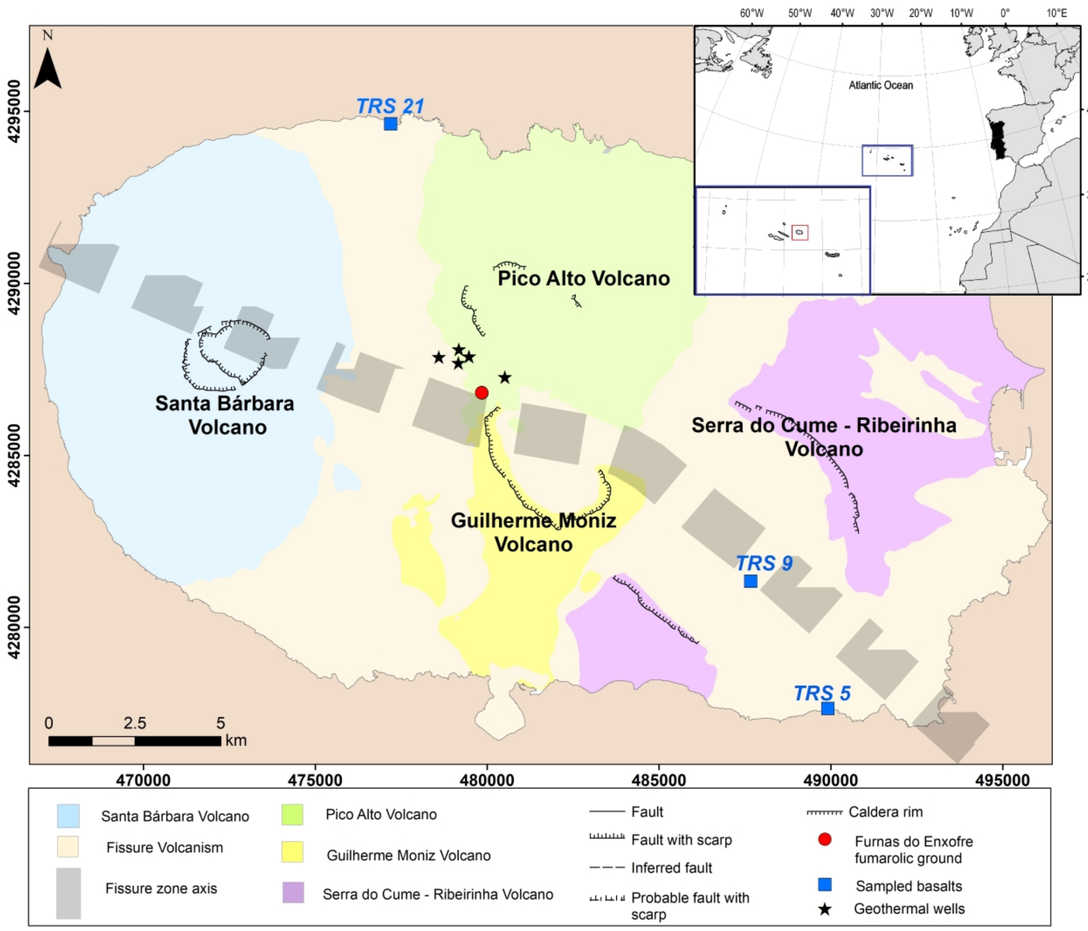

Figure 1

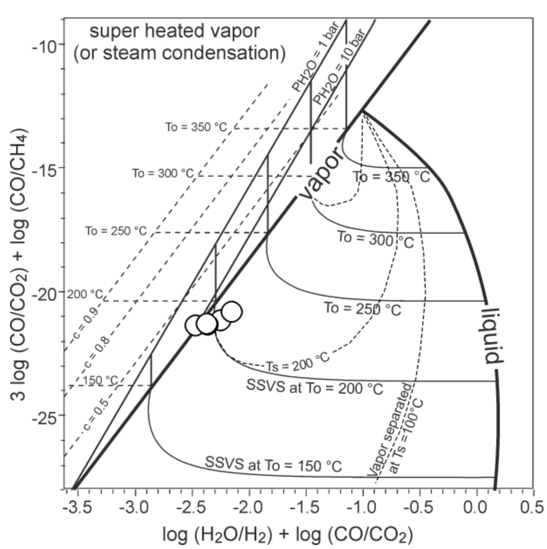

Figure 2

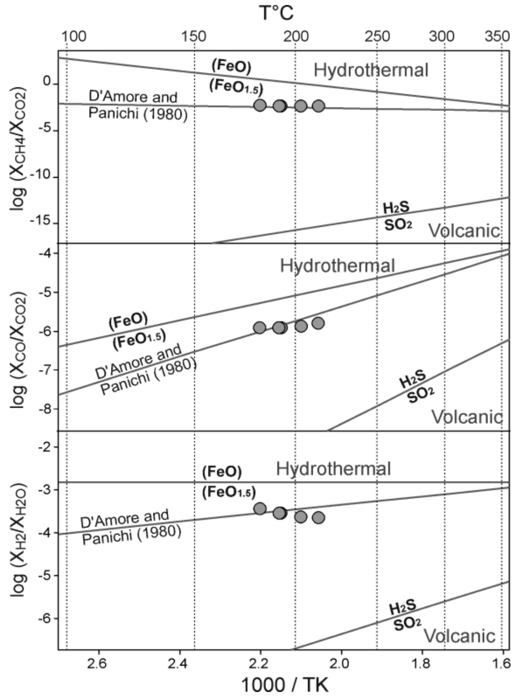

Figure 3

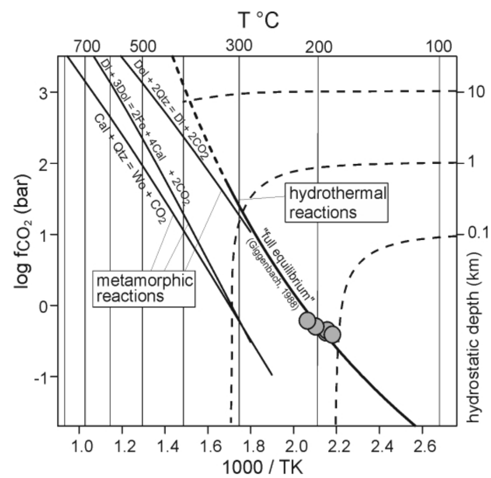

Figure 4

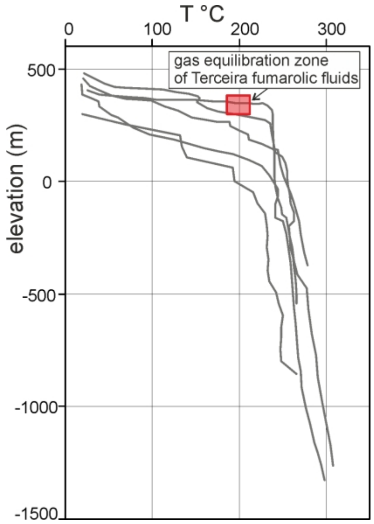

Figure 5

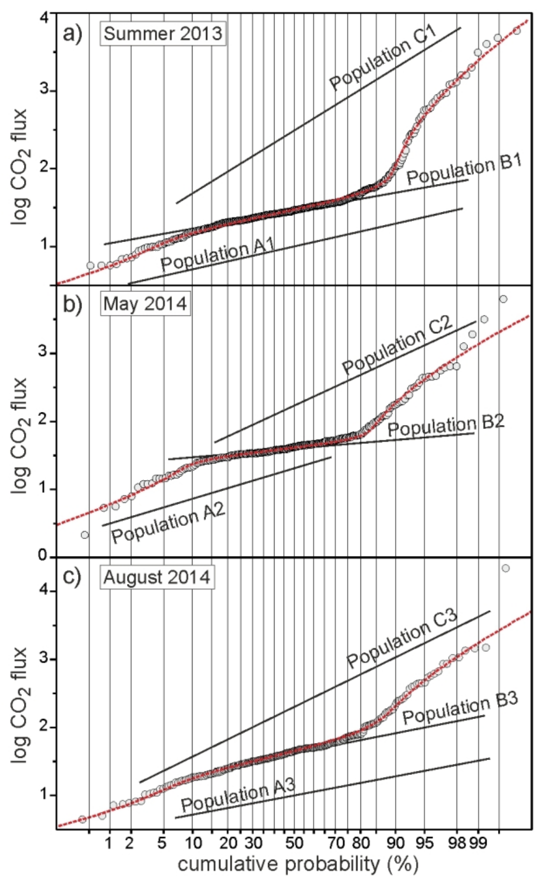

Figure 6

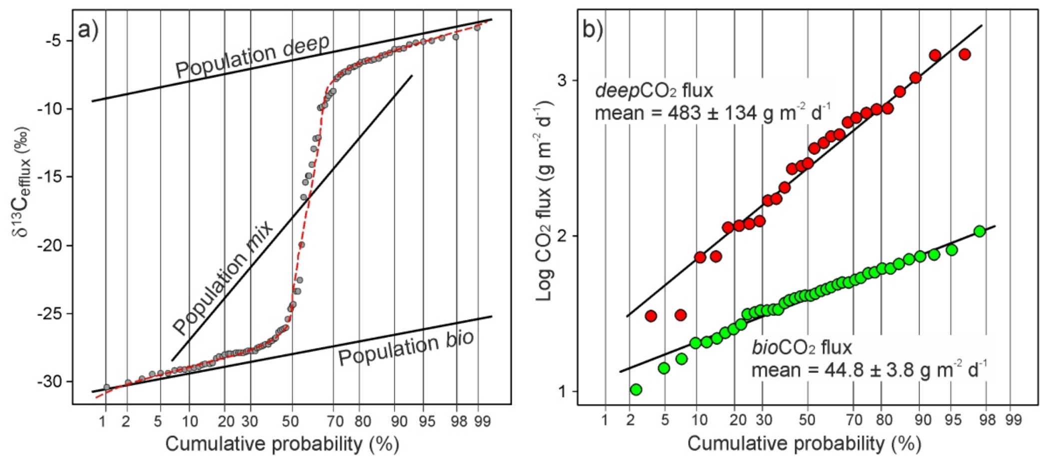

Figure 7

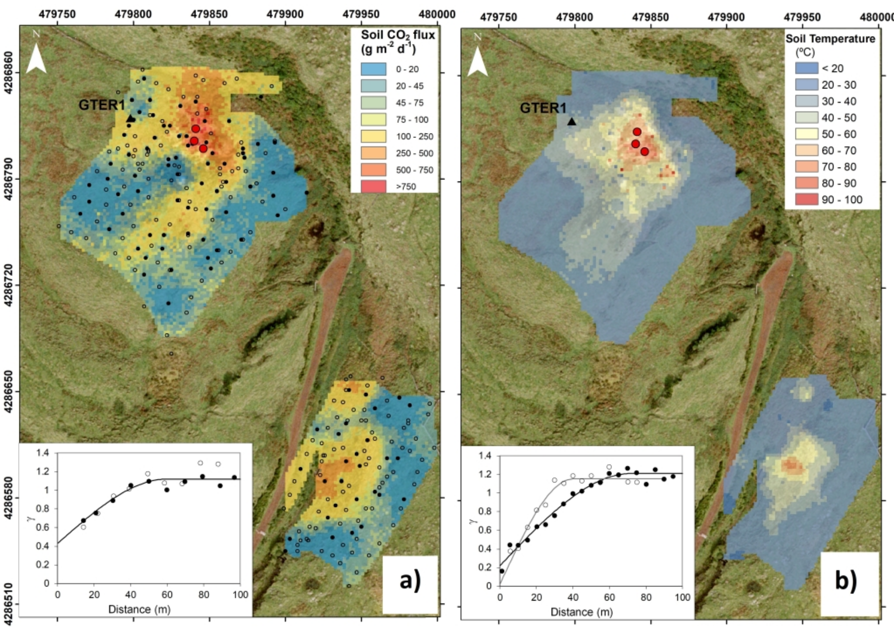

Figure 8

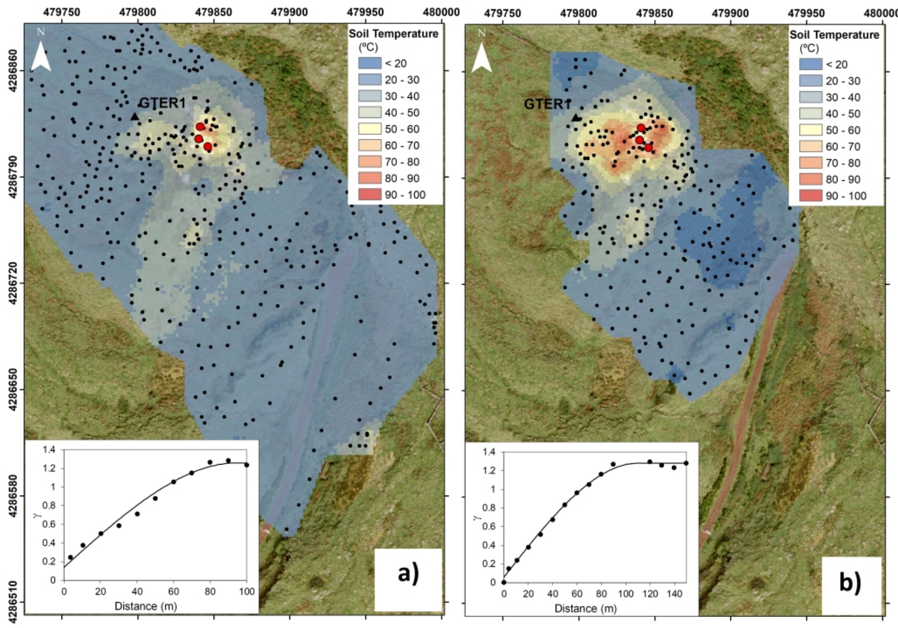
479750
479800
479850
479900
479950
480000
4286860
4286790
4286720
4286650
4286580
4286510
N
GTER1
Soil Temperature
(ºC)
< 20
20 - 30
30 - 40
40 - 50
50 - 60
60 - 70
70 - 80
80 - 90
90 - 100
γ
Distance (m)
a)
b)

Figure 9

Table 1

Gas emissions	UTM M	UTM P	Date	T (°C)	H_2O	CO_2	Stot	^{36}Ar	^{40}Ar	O_2	N_2	CH_4	H_2	He	CO
Furnas do Enxofre1	479846	4286810	04/10/2013	96.9	968318	30873	255	0.01	3.02	0.00	136	143	273	0.324	0.038
Furnas do Enxofre2	479841	4286823	04/10/2013	97.0	965072	34062	269	0.01	3.30	7.15	165	146	276	0.320	0.042
Furnas do Enxofre3	479840	4286815	04/10/2013	97.0	961715	37241	322	0.01	3.89	0.00	185	185	347	0.442	0.046
Furnas do Enxofre3	479840	4286815	26/08/2014	97.2	971953	27406	210	0.01	1.78	0.00	82	119	228	0.278	0.036
Furnas do Enxofre3	479840	4286815	26/08/2014	97.2	973195	26181	206	0.01	1.62	0.00	77	118	222	0.275	0.042

Table 2

Sample	Type	□^{15}N	□^{18}O	□D	□^{13}C	^{4}He/^{20}Ne	R/Ra	Rc/Ra
Furnas do Enxofre1	fumarole	-2.40	-8.26	-38.13	-4.48	31	9.51	9.60
Furnas do Enxofre2	fumarole	-1.85	-8.26	-38.13	-4.66	28	9.49	9.59
Furnas do Enxofre3	fumarole	-1.99	-8.26	-38.13	-4.66	28	9.49	9.59
Furnas do Enxofre3	fumarole	-0.51	*n.d.*	*n.d.*	-4.6	42	9.54	9.60
Furnas do Enxofre3	fumarole	-0.25	*n.d.*	*n.d.*	-4.27	*n.d.*	*n.d.*	*n.d.*
TRS 05 - Olivine	fluid inclusion	*n.d.*	*n.d.*	*n.d.*	-6.03	13	9.01	9.19
TRS 09 - Olivine	fluid inclusion	*n.d.*	*n.d.*	*n.d.*	-5.95	111	8.63	9.19
TRS 21 - Olivine	fluid inclusion	*n.d.*	*n.d.*	*n.d.*	-6.12	190	9.63	9.62

Table 3

Survey Ref.	Surveyed period	Variable	Number of measurements	Area (m^2)	Mean	Median	Minimum	Maximum	Standard deviation
S1	Summer 2013 (July/August)	Soil CO_2 flux (g m^{-2} d^{-1})	403	54783	124	29	0.15	5942	497
		Soil temperature (ºC)			28.9	24.3	18.3	99.5	11.6
		GTER1 CO_2 flux (g m^{-2} d^{-1})	39	-	219	222	165	267	26
S2	May/2014	Soil CO_2 flux (g m^{-2} d^{-1})	248	24957	123	42	2.14	6380	476
		Soil temperature (ºC)			33.8	23.9	17.3	99.8	18.2
		GTER1 CO_2 flux (g m^{-2} d^{-1})	17	-	110	104	86	157	18
S3	August/2014	Soil CO_2 flux (g m^{-2} d^{-1})	281	23715	179	45	4.45	21900	1316
		Soil temperature (ºC)	279		32.5	23.9	19.2	95.7	16.8
		$\delta^{13}C_{CO2}$ (‰ *vs*. PDB)	99		-18.83	-24.39	-30.41	-4.06	9.96
		GTER1 CO_2 flux (g m^{-2} d^{-1})	38	-	198	202	121	258	28

Table 4

Survey ref.	Sampled area (km^2)	Populations	Proportion (%)	Average ($g\ m^{-2}\ d^{-1}$)	Mean CO_2 90% Confidence Interval ($g\ m^{-2}\ d^{-1}$)	CO_2 output ($t\ d^{-1}$)	90% Confidence Interval ($t\ d^{-1}$)	CO_2 output ($t\ d^{-1}\ km^{-2}$)
S1	0.055	A1 - Biogenic	7	11.5	9.7 - 14.6	0.04	0.04 - 0.06	0.8
		B1 - Intermediate	80	31.4	29.7 - 33.5	1.38	1.30 - 1.47	25.1
		C1 - Deep	13	868	579 - 1556	6.18	4.13 - 11.08	112.8
S2	0.025	A2 - Biogenic	14	28.2	22.1 - 36.0	0.10	0.08 - 0.13	3.9
		B2 - Intermediate	65	40.9	39.5 - 42.5	0.66	0.64 - 0.69	26.6
		C2 - Deep	21	364	262 - 576	1.91	1.37 - 3.02	76.4
S3	0.024	A3 - Biogenic	6	11.4	9.3 - 15.4	0.02	0.01 - 0.02	0.7
		B3 - Intermediate	74	48.0	44.3 - 52.8	0.84	0.78 - 0.93	35.5
		C3 - Deep	20	466	328 - 765	2.21	1.55 - 3.63	93.2

Table 5

Q_{CO2} (kg s^{-1})	$R_{H2O/CO2}$ by weight	Q_{cond} (kg s^{-1})	$H_{v,100}$ (kJ kg^{-1})	$H_{L,20}$ (kJ kg^{-1})	QH_{cond} (kJ s^{-1})
0.0294	14.90	0.438	2676	83.96	1132

Declaration of interests

☐ The authors declare that they have no known competing financial interests or personal relationships that could have appeared to influence the work reported in this paper.

Fátima Viveiros
Giovanni Chiodini
Carlo Cardellini
Stefano Caliro
Vittorio Zanon
Catarina Silva
Andrea Luca Rizzo
Ana Hipólito
Lucía Moreno

Table A.1 - Soil CO_2 fluxes, temperature, A and B concentrations-isotopic compositions of data acquired during the surveys carried out at Furnas do Enxofre degassing area

Reference	UTM M	UTM P	Soil CO_2 flux ($g\ m^{-2}\ d^{-1}$)	Soil temperature (ºC)	Sampling date	$d^{13}C_{efflux}$ (‰ vs. V-PDB)	CO_2 concentration - A (ppm)	CO_2 concentration - B (ppm)
S1.1	479922	4286719	16.18	20.2	30/06/2013			
S1.2	479918	4286717	29.47	22.5	30/06/2013			
S1.3	479916	4286702	21.71	21.6	30/06/2013			
S1.4	479909	4286684	37.34	21.9	30/06/2013			
S1.5	479894	4286666	25.86	20.1	30/06/2013			
S1.6	479887	4286641	31.76	23.3	30/06/2013			
S1.7	479876	4286630	35.80	19.5	30/06/2013			
S1.8	479865	4286612	16.21	18.3	30/06/2013			
S1.9	479873	4286596	21.53	21.8	30/06/2013			
S1.10	479869	4286581	27.23	21.0	30/06/2013			
S1.11	479862	4286588	22.41	21.6	30/06/2013			
S1.12	479858	4286602	31.58	21.7	30/06/2013			
S1.13	479852	4286614	20.76	23.4	30/06/2013			
S1.14	479844	4286628	29.79	23.3	30/06/2013			
S1.15	479857	4286632	21.90	21.6	30/06/2013			
S1.16	479871	4286627	53.15	23.8	30/06/2013			
S1.17	479862	4286615	35.24	19.0	30/06/2013			
S1.18	479864	4286642	22.87	22.8	30/06/2013			
S1.19	479882	4286659	20.82	21.3	30/06/2013			
S1.20	479895	4286668	20.31	22.0	30/06/2013			
S1.21	479901	4286678	44.65	23.1	30/06/2013			
S1.22	479909	4286694	16.99	20.7	30/06/2013			
S1.23	479908	4286707	16.83	20.2	30/06/2013			

S1.24	479907	4286717	29.63	22.5	30/06/2013			
S1.25	479895	4286718	25.60	23.1	30/06/2013			
S1.26	479884	4286714	36.32	21.6	30/06/2013			
S1.27	479892	4286705	27.47	22.4	30/06/2013			
S1.28	479877	4286699	25.58	20.4	30/06/2013			
S1.29	479881	4286706	24.35	21.0	30/06/2013			
S1.30	479866	4286694	28.91	25.2	30/06/2013			
S1.31	479859	4286679	40.59	23.9	30/06/2013			
S1.32	479850	4286666	53.08	21.9	30/06/2013			
S1.33	479862	4286660	37.47	26.0	30/06/2013			
S1.34	479844	4286648	33.00	27.5	30/06/2013			
S1.35	479842	4286632	56.53	27.2	30/06/2013			
S1.36	479852	4286638	42.28	31.7	30/06/2013			
S1.37	479838	4286645	34.30	26.4	30/06/2013			
S1.38	479842	4286664	27.17	27.2	30/06/2013			
S1.39	479848	4286678	35.54	24.3	30/06/2013			
S1.40	479860	4286691	27.23	25.6	30/06/2013			
S1.41	479866	4286704	62.04	26.4	30/06/2013			
S1.42	479869	4286714	45.08	28.9	30/06/2013			
S1.43	479872	4286731	59.52	28.5	30/06/2013			
S1.44	479863	4286740	30.19	26.9	30/06/2013			
S1.45	479849	4286726	40.21	25.9	30/06/2013			
S1.46	479839	4286717	36.96	25.6	30/06/2013			
S1.47	479837	4286702	34.81	26.6	30/06/2013			
S1.48	479828	4286693	41.80	28.0	30/06/2013			
S1.49	479843	4286696	30.10	28.2	30/06/2013			
S1.50	479840	4286679	65.80	26.6	30/06/2013			
S1.51	479829	4286675	21.20	23.6	30/06/2013			
S1.52	479815	4286681	62.26	27.7	30/06/2013			

S1.53	479821	4286695	54.97	28.9	30/06/2013			
S1.54	479816	4286702	6.88	34.8	30/06/2013			
S1.55	479804	4286696	39.14	31.1	30/06/2013			
S1.56	479796	4286707	21.21	29.9	30/06/2013			
S1.57	479813	4286716	35.64	26.9	30/06/2013			
S1.58	479823	4286735	35.94	28.5	30/06/2013			
S1.59	479833	4286740	60.19	32.4	30/06/2013			
S1.60	479834	4286746	5941.59	57.5	30/06/2013			
S1.61	479837	4286746	56.43	34.4	30/06/2013			
S1.62	479840	4286749	38.49	35.8	30/06/2013			
S1.63	479839	4286752	1589.16	56.2	30/06/2013			
S1.64	479831	4286751	25.64	36.9	30/06/2013			
S1.65	479839	4286759	32.99	39.7	30/06/2013			
S1.66	479837	4286762	34.78	35.0	30/06/2013			
S1.67	479854	4286749	27.91	26.6	30/06/2013			
S1.68	479845	4286739	26.84	25.2	30/06/2013			
S1.69	479854	4286731	57.61	27.7	30/06/2013			
S1.70	479878	4286734	33.68	24.0	30/06/2013			
S1.71	479869	4286746	22.07	24.6	30/06/2013			
S1.72	479881	4286752	100.29	24.2	30/06/2013			
S1.73	479876	4286765	43.97	24.6	30/06/2013			
S1.74	479869	4286779	33.77	25.1	30/06/2013			
S1.75	479864	4286770	26.49	25.6	30/06/2013			
S1.76	479865	4286762	118.82	21.4	30/06/2013			
S1.77	479864	4286753	23.56	24.4	30/06/2013			
S1.78	479872	4286755	37.21	23.1	30/06/2013			
S1.79	479854	4286754	37.50	22.6	30/06/2013			
S1.80	479884	4286728	44.92	22.8	30/06/2013			
S1.81	479888	4286742	27.77	24.2	30/06/2013			

S1.82	479887	4286757	30.51	26.2	30/06/2013			
S1.83	479891	4286749	16.10	24.3	30/06/2013			
S1.84	479898	4286743	27.01	23.1	30/06/2013			
S1.85	479900	4286748	16.70	21.7	30/06/2013			
S1.86	479905	4286759	20.44	22.3	30/06/2013			
S1.87	479911	4286766	17.83	23.5	30/06/2013			
S1.88	479931	4286742	28.15	27.9	30/06/2013			
S1.89	479930	4286745	46.19	26.3	30/06/2013			
S1.90	479921	4286741	36.29	24.3	30/06/2013			
S1.91	479916	4286744	25.98	22.0	30/06/2013			
S1.92	479908	4286741	10.64	24.4	30/06/2013			
S1.93	479898	4286735	16.64	20.8	30/06/2013			
S1.94	479901	4286731	16.14	22.2	30/06/2013			
S1.95	479909	4286731	45.97	23.9	30/06/2013			
S1.96	479918	4286734	20.27	24.1	30/06/2013			
S1.97	479917	4286740	21.45	22.6	30/06/2013			
S1.98	479929	4286732	9.91	26.3	30/06/2013			
S1.99	479952	4286745	45.43	26.6	01/07/2013			
S1.100	479944	4286711	5.96	24.5	01/07/2013			
S1.101	479947	4286695	12.59	24.4	01/07/2013			
S1.102	479943	4286673	21.76	26.6	01/07/2013			
S1.103	479930	4286644	7.83	24.4	01/07/2013			
S1.104	479921	4286623	9.94	25.5	01/07/2013			
S1.105	479916	4286610	33.42	26.5	01/07/2013			
S1.106	479913	4286591	22.25	24.2	01/07/2013			
S1.107	479906	4286574	15.41	23.4	01/07/2013			
S1.108	479898	4286558	5.70	30.3	01/07/2013			
S1.109	479940	4286613	9.78	28.6	01/07/2013			
S1.110	479946	4286613	41.14	34.4	01/07/2013			

S1.111	479946	4286613	3115.90	53.2	01/07/2013			
S1.112	479946	4286613	13.05	36.6	01/07/2013			
S1.113	479945	4286621	15.55	25.9	01/07/2013			
S1.114	479951	4286621	349.66	55.3	01/07/2013			
S1.115	479951	4286620	112.29	43.8	01/07/2013			
S1.116	479950	4286613	23.77	41.0	01/07/2013			
S1.117	479946	4286630	9.82	22.1	01/07/2013			
S1.118	479953	4286641	11.40	24.5	01/07/2013			
S1.119	479960	4286651	12.76	22.4	01/07/2013			
S1.120	479966	4286658	10.89	19.5	01/07/2013			
S1.121	479965	4286670	20.64	24.1	01/07/2013			
S1.122	479969	4286680	11.48	21.0	01/07/2013			
S1.123	479794	4286818	35.38	25.8	02/07/2013			
S1.124	479793	4286809	31.89	37.8	02/07/2013			
S1.125	479800	4286818	697.35	38.5	02/07/2013			
S1.126	479801	4286825	21.39	37.5	02/07/2013			
S1.127	479808	4286827	1997.80	50.6	02/07/2013			
S1.128	479805	4286811	13.15	40.4	02/07/2013			
S1.129	479798	4286806	19.38	47.2	02/07/2013			
S1.130	479796	4286804	562.24	30.0	02/07/2013			
S1.131	479802	4286802	139.74	35.9	02/07/2013			
S1.132	479808	4286807	11.22	54.8	02/07/2013			
S1.133	479810	4286812	78.14	46.0	02/07/2013			
S1.134	479814	4286815	17.35	40.4	02/07/2013			
S1.135	479818	4286818	1303.61	45.6	02/07/2013			
S1.136	479807	4286815	54.07	55.3	02/07/2013			
S1.137	479808	4286806	64.40	48.4	02/07/2013			
S1.138	479807	4286802	94.98	30.4	02/07/2013			
S1.139	479808	4286798	12.49	19.8	02/07/2013			

S1.140	479814	4286808	15.91	44.8	02/07/2013			
S1.141	479820	4286812	172.28	34.1	02/07/2013			
S1.142	479822	4286817	1595.33	69.6	02/07/2013			
S1.143	479825	4286817	1238.17	52.5	02/07/2013			
S1.144	479824	4286816	8.75	35.8	02/07/2013			
S1.145	479823	4286808	12.17	22.8	02/07/2013			
S1.146	479828	4286811	925.03	75.7	02/07/2013			
S1.147	479832	4286814	14.20	39.3	02/07/2013			
S1.148	479830	4286816	65.67	27.1	02/07/2013			
S1.149	479829	4286820	108.74	33.2	02/07/2013			
S1.150	479825	4286823	56.59	34.7	02/07/2013			
S1.151	479831	4286823	0.15	23.9	02/07/2013			
S1.152	479830	4286821	5.73	27.0	02/07/2013			
S1.153	479836	4286818	156.39	45.7	02/07/2013			
S1.154	479842	4286822	217.24	95.9	02/07/2013			
S1.155	479845	4286827	813.85	67.4	02/07/2013			
S1.156	479845	4286833	281.20	40.5	02/07/2013			
S1.157	479846	4286834	14.27	40.1	02/07/2013			
S1.158	479846	4286840	453.46	46.3	02/07/2013			
S1.159	479838	4286842	36.75	42.1	02/07/2013			
S1.160	479837	4286842	950.87	46.1	02/07/2013			
S1.161	479846	4286835	35.50	26.2	02/07/2013			
S1.162	479845	4286826	108.69	56.6	02/07/2013			
S1.163	479843	4286822	4815.19	99.5	02/07/2013			
S1.164	479849	4286824	283.91	36.8	02/07/2013			
S1.165	479850	4286828	484.82	49.4	02/07/2013			
S1.166	479851	4286823	4021.88	92.2	02/07/2013			
S1.167	479852	4286823	83.64	62.1	02/07/2013			
S1.168	479848	4286821	281.57	73.9	02/07/2013			

S1.169	479842	4286814	316.36	38.3	02/07/2013			
S1.170	479839	4286810	426.67	59.4	02/07/2013			
S1.171	479831	4286806	15.47	42.9	02/07/2013			
S1.172	479837	4286804	7.05	36.1	02/07/2013			
S1.173	479845	4286809	738.24	50.1	02/07/2013			
S1.174	479851	4286811	111.06	65.7	02/07/2013			
S1.175	479847	4286807	865.68	91.1	02/07/2013			
S1.176	479841	4286802	42.72	42.0	02/07/2013			
S1.177	479841	4286798	7.26	28.7	02/07/2013			
S1.178	479824	4286805	577.00	51.2	02/07/2013			
S1.179	479825	4286800	12.80	48.3	02/07/2013			
S1.180	479829	4286797	20.29	57.5	02/07/2013			
S1.181	479827	4286797	19.64	46.7	02/07/2013			
S1.182	479870	4286773	26.31	23.4	02/07/2013			
S1.183	479871	4286783	29.30	32.8	02/07/2013			
S1.184	479868	4286776	17.47	30.4	02/07/2013			
S1.185	479864	4286782	1204.09	39.9	02/07/2013			
S1.186	479858	4286785	226.30	39.1	02/07/2013			
S1.187	479854	4286775	9.08	33.1	02/07/2013			
S1.188	479854	4286782	9.48	33.7	02/07/2013			
S1.189	479840	4286779	32.57	28.4	02/07/2013			
S1.190	479844	4286768	19.01	30.5	02/07/2013			
S1.191	479844	4286762	51.52	39.9	02/07/2013			
S1.192	479848	4286759	57.17	32.6	02/07/2013			
S1.193	479858	4286791	56.80	34.6	02/07/2013			
S1.194	479864	4286787	74.77	33.3	02/07/2013			
S1.195	479867	4286787	39.39	33.6	02/07/2013			
S1.196	479866	4286794	42.92	48.6	02/07/2013			
S1.197	479881	4286782	29.71	28.9	02/07/2013			

S1.198	479894	4286786	50.39	27.1	02/07/2013			
S1.199	479907	4286789	24.94	26.7	02/07/2013			
S1.200	479916	4286792	24.84	25.5	02/07/2013			
S1.201	479869	4286792	86.87	37.1	02/07/2013			
S1.202	479879	4286799	31.43	28.2	02/07/2013			
S1.203	479874	4286811	14.80	27.5	02/07/2013			
S1.204	479873	4286818	17.24	27.5	02/07/2013			
S1.205	479878	4286822	25.42	25.5	02/07/2013			
S1.206	479869	4286812	262.29	46.4	02/07/2013			
S1.207	479868	4286810	68.09	46.6	02/07/2013			
S1.208	479863	4286820	21.98	39.3	02/07/2013			
S1.209	479863	4286822	46.16	41.7	02/07/2013			
S1.210	479860	4286831	5.68	35.3	02/07/2013			
S1.211	479866	4286805	37.80	47.8	02/07/2013			
S1.212	479860	4286805	129.65	44.1	02/07/2013			
S1.213	479867	4286803	55.38	30.1	02/07/2013			
S1.214	479861	4286799	48.81	32.4	02/07/2013			
S1.215	479843	4286784	20.66	22.9	02/07/2013			
S1.216	479838	4286782	27.45	26.5	02/07/2013			
S1.217	479829	4286768	34.73	29.6	02/07/2013			
S1.218	479821	4286761	34.11	29.1	02/07/2013			
S1.219	479812	4286747	72.42	28.2	02/07/2013			
S1.220	479805	4286736	50.03	28.0	02/07/2013			
S1.221	479801	4286722	91.91	31.2	02/07/2013			
S1.222	479796	4286712	45.50	29.3	02/07/2013			
S1.223	479803	4286701	38.07	27.1	02/07/2013			
S1.224	479817	4286739	38.72	32.6	02/07/2013			
S1.225	479797	4286746	48.37	33.9	02/07/2013			
S1.226	479805	4286753	57.90	36.3	02/07/2013			

S1.227	479801	4286751	37.31	28.4	02/07/2013			
S1.228	479790	4286766	29.14	23.4	02/07/2013			
S1.229	479800	4286775	20.22	23.8	02/07/2013			
S1.230	479808	4286779	587.42	34.4	02/07/2013			
S1.231	479811	4286783	54.79	26.5	02/07/2013			
S1.232	479803	4286787	22.20	23.0	02/07/2013			
S1.233	479803	4286792	9.91	21.8	02/07/2013			
S1.234	479792	4286784	17.90	21.6	02/07/2013			
S1.235	479786	4286797	20.62	22.0	02/07/2013			
S1.236	479793	4286839	25.60	24.2	02/07/2013			
S1.237	479801	4286837	35.32	23.2	02/07/2013			
S1.238	479811	4286835	17.18	26.7	02/07/2013			
S1.239	479815	4286832	66.28	27.4	02/07/2013			
S1.240	479792	4286843	17.34	21.7	02/07/2013			
S1.241	479798	4286859	23.68	22.6	02/07/2013			
S1.242	479801	4286862	15.53	20.9	02/07/2013			
S1.243	479940	4286750	27.68	21.0	26/08/2013			
S1.244	479942	4286766	13.73	21.2	26/08/2013			
S1.245	479941	4286771	15.33	22.0	26/08/2013			
S1.246	479938	4286780	22.90	22.7	26/08/2013			
S1.247	479933	4286787	18.99	22.9	26/08/2013			
S1.248	479924	4286796	36.54	22.9	26/08/2013			
S1.249	479920	4286804	35.88	23.7	26/08/2013			
S1.250	479918	4286806	34.93	24.8	26/08/2013			
S1.251	479875	4286851	26.55	22.8	26/08/2013			
S1.252	479864	4286852	10.60	24.3	26/08/2013			
S1.253	479839	4286860	24.63	25.1	26/08/2013			
S1.254	479842	4286862	29.63	25.1	26/08/2013			
S1.255	479834	4286860	29.88	23.8	26/08/2013			

S1.256	479831	4286862	25.36	23.9	26/08/2013			
S1.257	479824	4286866	26.06	23.1	26/08/2013			
S1.258	479828	4286867	25.85	23.5	26/08/2013			
S1.259	479840	4286869	27.97	24.4	26/08/2013			
S1.260	479849	4286867	20.70	23.7	26/08/2013			
S1.261	479835	4286873	26.00	22.9	26/08/2013			
S1.262	479838	4286866	34.71	23.3	26/08/2013			
S1.263	479837	4286861	31.25	24.1	26/08/2013			
S1.264	479821	4286870	33.36	25.1	26/08/2013			
S1.265	479815	4286873	18.32	24.1	26/08/2013			
S1.266	479813	4286878	33.14	24.1	26/08/2013			
S1.267	479809	4286882	27.74	23.0	26/08/2013			
S1.268	479806	4286887	33.74	25.4	26/08/2013			
S1.269	479802	4286892	26.59	24.3	26/08/2013			
S1.270	479803	4286883	46.22	22.9	26/08/2013			
S1.271	479803	4286874	48.62	24.9	26/08/2013			
S1.272	479808	4286872	21.56	23.4	26/08/2013			
S1.273	479802	4286871	27.34	24.3	26/08/2013			
S1.274	479803	4286877	21.26	22.4	26/08/2013			
S1.275	479800	4286880	27.37	21.6	26/08/2013			
S1.276	479802	4286891	41.80	24.1	26/08/2013			
S1.277	479796	4286886	17.58	24.0	26/08/2013			
S1.278	479791	4286862	41.49	23.1	26/08/2013			
S1.279	479792	4286855	30.03	22.7	26/08/2013			
S1.280	479790	4286846	37.39	23.9	26/08/2013			
S1.281	479789	4286837	23.96	25.0	26/08/2013			
S1.282	479788	4286828	33.45	23.0	26/08/2013			
S1.283	479787	4286818	40.60	33.9	26/08/2013			
S1.284	479786	4286811	83.33	34.0	26/08/2013			

S1.285	479783	4286806	25.30	30.4	26/08/2013			
S1.286	479782	4286801	24.25	30.0	26/08/2013			
S1.287	479775	4286800	12.35	24.1	26/08/2013			
S1.288	479775	4286805	26.14	25.4	26/08/2013			
S1.289	479777	4286809	25.82	26.1	26/08/2013			
S1.290	479781	4286816	31.78	24.0	26/08/2013			
S1.291	479784	4286830	32.62	22.9	26/08/2013			
S1.292	479780	4286835	19.17	22.3	26/08/2013			
S1.293	479786	4286840	33.14	22.7	26/08/2013			
S1.294	479784	4286851	33.26	22.8	26/08/2013			
S1.295	479785	4286861	31.41	21.4	26/08/2013			
S1.296	479780	4286863	35.43	22.5	26/08/2013			
S1.297	479777	4286855	25.90	23.6	26/08/2013			
S1.298	479769	4286852	27.95	23.5	26/08/2013			
S1.299	479769	4286860	34.68	24.2	26/08/2013			
S1.300	479764	4286872	31.10	24.2	26/08/2013			
S1.301	479759	4286866	32.44	24.0	26/08/2013			
S1.302	479760	4286856	26.66	23.2	26/08/2013			
S1.303	479761	4286846	28.97	23.7	26/08/2013			
S1.304	479759	4286838	28.13	23.2	26/08/2013			
S1.305	479757	4286828	19.37	23.2	26/08/2013			
S1.306	479769	4286825	32.17	23.8	26/08/2013			
S1.307	479776	4286823	32.84	23.4	26/08/2013			
S1.308	479767	4286822	30.78	24.1	26/08/2013			
S1.309	479764	4286813	33.42	23.9	26/08/2013			
S1.310	479772	4286813	24.85	23.2	26/08/2013			
S1.311	479758	4286817	27.45	24.9	26/08/2013			
S1.312	479758	4286826	21.31	22.8	26/08/2013			
S1.313	479758	4286838	38.62	22.3	26/08/2013			

S1.314	479757	4286851	24.41	23.4	26/08/2013			
S1.315	479755	4286866	42.28	23.4	26/08/2013			
S1.316	479752	4286873	22.47	23.0	26/08/2013			
S1.317	479755	4286881	25.50	24.6	26/08/2013			
S1.318	479739	4286872	20.60	23.9	26/08/2013			
S1.319	479738	4286864	28.22	23.7	26/08/2013			
S1.320	479737	4286850	23.30	22.1	26/08/2013			
S1.321	479750	4286846	26.12	23.1	26/08/2013			
S1.322	479738	4286844	26.40	22.0	26/08/2013			
S1.323	479744	4286829	27.68	23.2	26/08/2013			
S1.324	479745	4286817	22.18	22.1	26/08/2013			
S1.325	479741	4286804	14.83	23.0	26/08/2013			
S1.326	479734	4286797	32.67	23.6	26/08/2013			
S1.327	479724	4286788	24.65	24.8	26/08/2013			
S1.328	479738	4286821	33.67	23.0	26/08/2013			
S1.329	479729	4286834	31.79	24.0	26/08/2013			
S1.330	479730	4286854	36.79	23.7	26/08/2013			
S1.331	479730	4286860	23.78	22.3	26/08/2013			
S1.332	479721	4286881	17.03	25.8	26/08/2013			
S1.333	479729	4286892	26.04	24.1	26/08/2013			
S1.334	479766	4286800	31.03	22.2	26/08/2013			
S1.335	479768	4286798	23.04	20.5	26/08/2013			
S1.336	479773	4286795	28.13	21.8	26/08/2013			
S1.337	479782	4286789	31.11	22.8	26/08/2013			
S1.338	479782	4286782	30.26	22.7	26/08/2013			
S1.339	479781	4286774	28.13	21.8	26/08/2013			
S1.340	479773	4286774	33.35	21.9	26/08/2013			
S1.341	479776	4286782	29.97	22.1	26/08/2013			
S1.342	479772	4286790	22.53	21.6	26/08/2013			

S1.343	479765	4286791	23.52	22.1	26/08/2013			
S1.344	479757	4286786	28.21	21.6	26/08/2013			
S1.345	479752	4286779	21.61	19.8	26/08/2013			
S1.346	479762	4286777	30.36	21.7	26/08/2013			
S1.347	479764	4286770	26.37	20.8	26/08/2013			
S1.348	479753	4286771	34.75	21.3	26/08/2013			
S1.349	479748	4286776	46.42	19.5	26/08/2013			
S1.350	479749	4286783	23.27	19.9	26/08/2013			
S1.351	479744	4286789	26.42	20.8	26/08/2013			
S1.352	479736	4286785	27.77	22.2	26/08/2013			
S1.353	479739	4286780	36.13	21.4	26/08/2013			
S1.354	479737	4286769	24.13	19.1	26/08/2013			
S1.355	479787	4286747	36.19	26.1	27/08/2013			
S1.356	479782	4286747	19.68	22.8	27/08/2013			
S1.357	479780	4286753	26.76	21.5	27/08/2013			
S1.358	479786	4286762	22.27	20.8	27/08/2013			
S1.359	479774	4286762	33.02	21.1	27/08/2013			
S1.360	479776	4286776	23.72	21.8	27/08/2013			
S1.361	479766	4286780	56.49	21.0	27/08/2013			
S1.362	479767	4286784	24.14	20.1	27/08/2013			
S1.363	479756	4286767	29.46	20.6	27/08/2013			
S1.364	479763	4286758	16.36	21.4	27/08/2013			
S1.365	479753	4286754	37.57	21.8	27/08/2013			
S1.366	479756	4286740	22.94	22.1	27/08/2013			
S1.367	479762	4286731	30.62	22.1	27/08/2013			
S1.368	479777	4286723	18.38	22.2	27/08/2013			
S1.369	479777	4286733	26.07	21.9	27/08/2013			
S1.370	479783	4286737	31.13	21.6	27/08/2013			
S1.371	479747	4286758	11.57	21.1	27/08/2013			

S1.372	479747	4286764	29.71	21.2	27/08/2013			
S1.373	479798	4286873	22.79	22.3	27/08/2013			
S1.374	479788	4286873	29.66	20.4	27/08/2013			
S1.375	479786	4286873	27.59	20.9	27/08/2013			
S1.376	479778	4286882	24.72	20.8	27/08/2013			
S1.377	479782	4286882	20.15	21.4	27/08/2013			
S1.378	479784	4286881	13.11	19.9	27/08/2013			
S1.379	479794	4286878	20.39	20.1	27/08/2013			
S1.380	479944	4286752	18.20	20.5	27/08/2013			
S1.381	479952	4286746	17.82	20.9	27/08/2013			
S1.382	479963	4286740	21.18	21.6	27/08/2013			
S1.383	479973	4286734	23.82	22.4	27/08/2013			
S1.384	479984	4286727	21.49	21.5	27/08/2013			
S1.385	479992	4286712	19.79	22.4	27/08/2013			
S1.386	479989	4286706	21.26	23.0	27/08/2013			
S1.387	479986	4286708	26.66	22.7	27/08/2013			
S1.388	479992	4286700	21.58	25.4	27/08/2013			
S1.389	479995	4286694	32.62	23.9	27/08/2013			
S1.390	479995	4286691	33.08	30.0	27/08/2013			
S1.391	479996	4286687	73.11	25.3	27/08/2013			
S1.392	479995	4286680	53.69	27.3	27/08/2013			
S1.393	479996	4286694	610.74	35.2	27/08/2013			
S1.394	479996	4286700	29.48	27.6	27/08/2013			
S1.395	479990	4286732	34.72	26.2	27/08/2013			
S1.396	479986	4286738	39.76	27.8	27/08/2013			
S1.397	479976	4286750	61.59	26.6	27/08/2013			
S1.398	479971	4286754	31.18	21.5	27/08/2013			
S1.399	479969	4286760	24.65	24.2	27/08/2013			
S1.400	479960	4286771	21.73	24.4	27/08/2013			

S1.401	479960	4286767	31.59	23.8	27/08/2013			
S1.402	479962	4286759	23.88	25.4	27/08/2013			
S1.403	479969	4286747	20.77	22.0	27/08/2013			
S2.1	479925	4286724	14.59	23.2	30/05/2014			
S2.2	479879	4286735	14.59	19.2	30/05/2014			
S2.3	479870	4286742	39.57	17.8	30/05/2014			
S2.4	479857	4286753	33.08	20.7	30/05/2014			
S2.5	479864	4286761	32.63	19.0	30/05/2014			
S2.6	479867	4286773	16.70	22.3	30/05/2014			
S2.7	479870	4286791	29.34	35.1	30/05/2014			
S2.8	479876	4286767	39.06	18.0	30/05/2014			
S2.9	479883	4286754	30.91	17.6	30/05/2014			
S2.10	479882	4286746	24.84	18.5	30/05/2014			
S2.11	479875	4286748	47.07	17.6	30/05/2014			
S2.12	479866	4286757	35.01	19.6	30/05/2014			
S2.13	479866	4286783	62.05	46.6	30/05/2014			
S2.14	479869	4286788	104.56	40.7	30/05/2014			
S2.15	479865	4286797	61.05	40.5	30/05/2014			
S2.16	479863	4286798	110.06	44.2	30/05/2014			
S2.17	479864	4286787	45.05	45.7	30/05/2014			
S2.18	479858	4286790	67.00	44.2	30/05/2014			
S2.19	479857	4286784	22.01	30.6	30/05/2014			
S2.20	479854	4286775	12.12	29.7	30/05/2014			
S2.21	479850	4286772	29.72	27.6	30/05/2014			
S2.22	479842	4286772	33.64	30.6	30/05/2014			
S2.23	479848	4286763	38.40	38.3	30/05/2014			
S2.24	479854	4286771	73.82	36.1	30/05/2014			
S2.25	479841	4286779	63.89	29.7	30/05/2014			
S2.26	479844	4286785	38.34	26.5	30/05/2014			

S2.27	479835	4286779	39.25	28.5	30/05/2014			
S2.28	479817	4286758	68.62	38.4	30/05/2014			
S2.29	479814	4286757	42.29	43.7	30/05/2014			
S2.30	479809	4286769	51.99	31.9	30/05/2014			
S2.31	479805	4286753	55.82	38.1	30/05/2014			
S2.32	479799	4286754	26.77	29.6	30/05/2014			
S2.33	479791	4286765	51.46	21.4	30/05/2014			
S2.34	479796	4286773	41.13	22.1	30/05/2014			
S2.35	479804	4286781	37.61	21.8	30/05/2014			
S2.36	479809	4286779	35.65	34.0	30/05/2014			
S2.37	479812	4286784	121.68	34.4	30/05/2014			
S2.38	479803	4286780	50.80	21.9	30/05/2014			
S2.39	479804	4286792	41.13	23.4	30/05/2014			
S2.40	479892	4286785	14.47	20.8	30/05/2014			
S2.41	479789	4286795	59.09	22.2	30/05/2014			
S2.42	479796	4286797	38.84	34.0	30/05/2014			
S2.43	479802	4286799	212.91	33.7	30/05/2014			
S2.44	479790	4286802	76.99	36.0	30/05/2014			
S2.45	479792	4286812	56.85	36.0	30/05/2014			
S2.46	479799	4286811	64.74	56.2	30/05/2014			
S2.47	479801	4286806	156.18	57.4	30/05/2014			
S2.48	479805	4286812	58.00	65.2	30/05/2014			
S2.49	479804	4286803	51.24	60.3	30/05/2014			
S2.50	479806	4286803	461.65	60.5	30/05/2014			
S2.51	479810	4286805	7.86	57.8	30/05/2014			
S2.52	479809	4286812	31.86	65.2	30/05/2014			
S2.53	479814	4286817	14.60	55.4	30/05/2014			
S2.54	479817	4286817	17.35	52.4	30/05/2014			
S2.55	479818	4286821	104.34	72.1	30/05/2014			

S2.56	479822	4286820	162.29	82.9	30/05/2014			
S2.57	479819	4286813	1883.66	60.5	30/05/2014			
S2.58	479816	4286812	50.98	57.5	30/05/2014			
S2.59	479826	4286807	11.91	70.1	30/05/2014			
S2.60	479825	4286806	439.24	79.8	30/05/2014			
S2.61	479824	4286801	563.47	53.3	30/05/2014			
S2.62	479823	4286798	10.72	64.2	30/05/2014			
S2.63	479823	4286798	25.92	98.2	30/05/2014			
S2.64	479833	4286807	20.46	54.8	30/05/2014			
S2.65	479836	4286810	84.66	91.4	30/05/2014			
S2.66	479830	4286814	644.20	92.5	30/05/2014			
S2.67	479834	4286817	457.25	78.9	30/05/2014			
S2.68	479838	4286820	466.52	43.1	30/05/2014			
S2.69	479842	4286824	55.90	82.6	30/05/2014			
S2.70	479841	4286830	1272.55	45.0	30/05/2014			
S2.71	479844	4286832	247.07	48.0	30/05/2014			
S2.72	479847	4286836	192.10	38.8	30/05/2014			
S2.73	479846	4286841	15.99	51.7	30/05/2014			
S2.74	479837	4286843	197.59	49.6	30/05/2014			
S2.75	479848	4286831	170.38	47.9	30/05/2014			
S2.76	479849	4286827	649.74	67.5	30/05/2014			
S2.77	479852	4286830	315.15	62.7	30/05/2014			
S2.78	479851	4286824	130.47	81.3	30/05/2014			
S2.79	479855	4286824	332.40	99.8	30/05/2014			
S2.80	479845	4286822	622.79	65.3	30/05/2014			
S2.81	479847	4286823	437.65	66.1	30/05/2014			
S2.82	479843	4286820	180.12	57.3	30/05/2014			
S2.83	479848	4286813	58.89	77.0	30/05/2014			
S2.84	479849	4286807	193.83	91.5	30/05/2014			

S2.85	479843	4286801	6380.08	50.1	30/05/2014			
S2.86	479842	4286809	16.73	73.8	30/05/2014			
S2.87	479838	4286804	15.83	64.8	30/05/2014			
S2.88	479840	4286810	5.67	69.4	30/05/2014			
S2.89	479843	4286813	242.29	41.3	30/05/2014			
S2.90	479836	4286818	3158.52	49.6	30/05/2014			
S2.91	479813	4286821	299.25	53.7	30/05/2014			
S2.92	479808	4286820	2.14	52.5	30/05/2014			
S2.93	479804	4286825	46.38	49.3	30/05/2014			
S2.94	479808	4286827	118.10	59.2	30/05/2014			
S2.95	479801	4286829	94.16	49.6	30/05/2014			
S2.96	479798	4286822	18.62	44.4	30/05/2014			
S2.97	479793	4286824	7.22	33.5	30/05/2014			
S2.98	479794	4286841	48.26	24.0	30/05/2014			
S2.99	479802	4286836	43.67	23.8	30/05/2014			
S2.100	479811	4286837	34.34	30.6	30/05/2014			
S2.101	479819	4286841	37.49	31.1	30/05/2014			
S2.102	479815	4286841	49.37	41.0	30/05/2014			
S2.103	479792	4286848	36.09	19.0	30/05/2014			
S2.104	479794	4286855	39.06	19.7	30/05/2014			
S2.105	479798	4286863	27.94	18.6	30/05/2014			
S2.106	479808	4286859	34.56	19.7	30/05/2014			
S2.107	479804	4286850	38.04	21.4	30/05/2014			
S2.108	479830	4286861	29.64	21.2	30/05/2014			
S2.109	479873	4286849	35.04	19.8	30/05/2014			
S2.110	479935	4286745	26.03	20.7	30/05/2014			
S2.111	479929	4286750	43.33	29.3	30/05/2014			
S2.112	479919	4286743	5.43	18.9	30/05/2014			
S2.113	479915	4286739	37.73	18.0	30/05/2014			

S2.114	479908	4286739	31.43	19.7	30/05/2014			
S2.115	479900	4286736	34.89	17.3	30/05/2014			
S2.116	479904	4286734	31.51	18.0	30/05/2014			
S2.117	479910	4286734	24.74	19.1	30/05/2014			
S2.118	479915	4286739	27.71	19.4	30/05/2014			
S2.119	479914	4286732	63.13	20.6	30/05/2014			
S2.120	479898	4286726	33.31	18.7	30/05/2014			
S2.121	479890	4286725	33.14	17.6	30/05/2014			
S2.122	479883	4286723	39.50	18.4	31/05/2014			
S2.123	479885	4286730	45.27	18.3	31/05/2014			
S2.124	479889	4286738	35.59	17.8	31/05/2014			
S2.125	479886	4286747	39.02	19.0	31/05/2014			
S2.126	479895	4286747	35.49	18.9	31/05/2014			
S2.127	479895	4286741	26.52	17.3	31/05/2014			
S2.128	479898	4286750	44.69	19.6	31/05/2014			
S2.129	479801	4286760	48.26	20.2	31/05/2014			
S2.130	479908	4286773	41.74	19.2	31/05/2014			
S2.131	479915	4286780	42.33	20.3	31/05/2014			
S2.132	479912	4286785	45.34	18.6	31/05/2014			
S2.133	479904	4286787	24.38	20.3	31/05/2014			
S2.134	479905	4286776	45.39	19.4	31/05/2014			
S2.135	479901	4286765	32.44	19.5	31/05/2014			
S2.136	479892	4286759	37.32	20.1	31/05/2014			
S2.137	479889	4286772	34.18	20.1	31/05/2014			
S2.138	479888	4286780	48.20	20.4	31/05/2014			
S2.139	479880	4286782	29.63	21.3	31/05/2014			
S2.140	479887	4286788	34.20	21.4	31/05/2014			
S2.141	479884	4286798	34.53	22.2	31/05/2014			
S2.142	479875	4286794	51.50	32.0	31/05/2014			

S2.143	479876	4286785	36.13	23.6	31/05/2014			
S2.144	479871	4286792	33.50	55.1	31/05/2014			
S2.145	479874	4286796	371.70	37.8	31/05/2014			
S2.146	479877	4286801	74.17	24.4	31/05/2014			
S2.147	479872	4286806	37.66	29.7	31/05/2014			
S2.148	479869	4286799	34.12	46.4	31/05/2014			
S2.149	479863	4286801	84.56	42.3	31/05/2014			
S2.150	479868	4286805	61.64	34.6	31/05/2014			
S2.151	479857	4286805	27.88	40.9	31/05/2014			
S2.152	479875	4286810	83.66	23.9	31/05/2014			
S2.153	479871	4286816	32.13	36.8	31/05/2014			
S2.154	479868	4286812	89.46	58.7	31/05/2014			
S2.155	479872	4286821	34.30	30.3	31/05/2014			
S2.156	479862	4286822	34.14	54.1	31/05/2014			
S2.157	479860	4286829	54.33	35.1	31/05/2014			
S2.158	479880	4286769	46.90	22.3	31/05/2014			
S2.159	479886	4286757	44.18	20.6	31/05/2014			
S2.160	479887	4286745	35.40	22.5	31/05/2014			
S2.161	479854	4286748	43.78	21.6	31/05/2014			
S2.162	479845	4286740	53.93	21.0	31/05/2014			
S2.163	479838	4286735	21.51	21.7	31/05/2014			
S2.164	479834	4286745	53.97	40.2	31/05/2014			
S2.165	479837	4286752	42.51	50.7	31/05/2014			
S2.166	479841	4286747	62.67	43.2	31/05/2014			
S2.167	479845	4286753	52.24	43.9	31/05/2014			
S2.168	479845	4286759	121.13	31.2	31/05/2014			
S2.169	479838	4286763	33.27	54.3	31/05/2014			
S2.170	479839	4286768	174.86	45.0	31/05/2014			
S2.171	479832	4286765	124.07	45.2	31/05/2014			

S2.172	479835	4286775	98.58	33.9	31/05/2014			
S2.173	479826	4286764	46.35	29.5	31/05/2014			
S2.174	479816	4286754	29.51	31.8	31/05/2014			
S2.175	479822	4286750	36.44	38.3	31/05/2014			
S2.176	479814	4286747	62.02	26.7	31/05/2014			
S2.177	479805	4286735	53.04	27.6	31/05/2014			
S2.178	479800	4286730	33.88	27.0	31/05/2014			
S2.179	479791	4286718	48.35	26.0	31/05/2014			
S2.180	479805	4286713	36.64	23.3	31/05/2014			
S2.181	479814	4286726	57.62	24.1	31/05/2014			
S2.182	479819	4286741	52.16	38.4	31/05/2014			
S2.183	479823	4286747	35.54	41.3	31/05/2014			
S2.184	479830	4286736	96.87	26.3	31/05/2014			
S2.185	479821	4286718	61.46	26.3	31/05/2014			
S2.186	479812	4286706	52.58	24.4	31/05/2014			
S2.187	479810	4286697	50.47	22.5	31/05/2014			
S2.188	479822	4286691	57.57	22.7	31/05/2014			
S2.189	479826	4286704	36.95	23.1	31/05/2014			
S2.190	479832	4286704	31.41	21.7	31/05/2014			
S2.191	479841	4286709	54.27	23.5	31/05/2014			
S2.192	479843	4286722	50.55	21.2	31/05/2014			
S2.193	479853	4286728	51.58	27.2	31/05/2014			
S2.194	479857	4286740	55.52	23.7	31/05/2014			
S2.195	479862	4286744	55.96	21.8	31/05/2014			
S2.196	479869	4286737	32.99	22.7	31/05/2014			
S2.197	479860	4286724	46.22	22.3	31/05/2014			
S2.198	479846	4286714	38.36	23.5	31/05/2014			
S2.199	479837	4286699	44.74	22.3	31/05/2014			
S2.200	479837	4286690	29.07	23.7	31/05/2014			

S2.201	479848	4286703	41.43	22.7	31/05/2014			
S2.202	479859	4286722	39.21	23.8	31/05/2014			
S2.203	479865	4286729	59.28	22.8	31/05/2014			
S2.204	479870	4286736	42.86	23.1	31/05/2014			
S2.205	479878	4286725	31.22	23.2	31/05/2014			
S2.206	479868	4286718	27.29	24.0	31/05/2014			
S2.207	479858	4286706	47.97	22.7	31/05/2014			
S2.208	479844	4286681	44.36	22.8	31/05/2014			
S2.209	479853	4286681	43.69	21.7	31/05/2014			
S2.210	479866	4286696	42.82	22.0	31/05/2014			
S2.211	479874	4286707	33.32	22.6	31/05/2014			
S2.212	479886	4286716	49.54	22.0	31/05/2014			
S2.213	479894	4286713	33.67	21.3	31/05/2014			
S2.214	479883	4286703	35.37	19.5	31/05/2014			
S2.215	479875	4286693	19.68	21.1	31/05/2014			
S2.216	479868	4286688	44.78	21.4	31/05/2014			
S2.217	479857	4286686	33.14	21.4	31/05/2014			
S2.218	479843	4286685	32.75	20.7	31/05/2014			
S2.219	479840	4286676	26.36	21.2	31/05/2014			
S2.220	479854	4286679	26.95	21.0	31/05/2014			
S2.221	479855	4286670	22.93	20.5	31/05/2014			
S2.222	479847	4286661	32.52	24.0	31/05/2014			
S2.223	479861	4286668	26.05	20.2	31/05/2014			
S2.224	479863	4286660	46.53	18.2	31/05/2014			
S2.225	479872	4286668	29.64	20.2	31/05/2014			
S2.226	479881	4286663	44.32	23.3	31/05/2014			
S2.227	479870	4286658	41.95	21.3	31/05/2014			
S2.228	479873	4286648	43.87	20.7	31/05/2014			
S2.229	479883	4286655	33.75	20.3	31/05/2014			

S2.230	479890	4286660	41.61	20.9	31/05/2014			
S2.231	479898	4286666	45.39	21.0	31/05/2014			
S2.232	479906	4286675	35.61	20.8	31/05/2014			
S2.233	479910	4286683	51.63	20.7	31/05/2014			
S2.234	479914	4286696	55.87	20.6	31/05/2014			
S2.235	479917	4286702	20.78	23.0	31/05/2014			
S2.236	479910	4286699	47.32	20.4	31/05/2014			
S2.237	479899	4286691	39.84	19.6	31/05/2014			
S2.238	479898	4286679	46.16	21.3	31/05/2014			
S2.239	479917	4286714	40.70	20.7	31/05/2014			
S2.240	479907	4286720	45.41	19.8	31/05/2014			
S2.241	479941	4286749	39.65	20.9	31/05/2014			
S2.242	479942	4286759	14.58	19.9	31/05/2014			
S2.243	479939	4286770	12.33	22.4	31/05/2014			
S2.244	479922	4286797	21.11	18.6	31/05/2014			
S2.245	479914	4286805	28.97	20.7	31/05/2014			
S2.246	479828	4286858	27.68	21.7	31/05/2014			
S2.247	479804	4286868	38.68	18.8	31/05/2014			
S2.248	479798	4286868	33.51	19.5	31/05/2014			
S3.1	479794	4286819	45.00	31.5	26/08/2014	-14.92	832	1016
S3.2	479809	4286810	35.59	47.5	26/08/2014	-8.85	752	974
S3.3	479823	4286799	246.04	56.0	26/08/2014	-9.21	1180	1203
S3.4	479828	4286804	4.45	47.5	26/08/2014	-16.50	645	606
S3.5	479814	4286817	30.61	43.1	26/08/2014	-7.48	726	902
S3.6	479800	4286829	26.24	43.2	26/08/2014	-8.69	649	737
S3.7	479799	4286842	10.34	21.8	26/08/2014	-30.08	585	607
S3.8	479807	4286856	25.39	21.7	26/08/2014	-24.39	697	810
S3.9	479811	4286842	32.02	23.6	26/08/2014	-29.19	705	745
S3.10	479820	4286825	185.08	54.5	26/08/2014	-14.87	1647	1946

S3.11	479836	4286812	1487.12	87.3	26/08/2014	-5.90	7554	2791
S3.12	479849	4286800	18.33	44.3	26/08/2014	-24.68	626	761
S3.13	479848	4286814	397.93	88.0	27/08/2014	-5.56	1628	2478
S3.14	479841	4286816	106.67	52.6	27/08/2014			
S3.15	479830	4286818	39.67	31.6	27/08/2014	-22.59	710	986
S3.16	479822	4286821	103.02	37.2	27/08/2014			
S3.17	479847	4286828	1452.97	50.0	27/08/2014	-5.09	4768	8992
S3.18	479851	4286820	433.79	87.3	27/08/2014			
S3.19	479842	4286833	140.34	82.6	27/08/2014			
S3.20	479831	4286838	31.22	38.2	27/08/2014	-6.90	865	999
S3.21	479848	4286836	18.75	58.5	27/08/2014			
S3.22	479841	4286841	580.00	48.6	27/08/2014	-5.30	2561	3583
S3.23	479833	4286844	404.58	60.1	27/08/2014			
S3.24	479842	4286844	43.41	51.6	27/08/2014			
S3.25	479790	4286810	45.00	31.8	27/08/2014			
S3.26	479804	4286796	57.83	33.5	27/08/2014			
S3.27	479797	4286806	24.25	30.3	27/08/2014	-23.39	695	884
S3.28	479825	4286789	7.76	33.8	27/08/2014			
S3.29	479785	4286800	32.08	27.0	27/08/2014	-26.83	696	1001
S3.30	479793	4286796	135.45	32.7	27/08/2014			
S3.31	479801	4286792	49.48	23.9	27/08/2014	-26.20	701	1013
S3.32	479810	4286790	25.03	28.0	27/08/2014			
S3.33	479776	4286795	32.08	20.6	27/08/2014			
S3.34	479783	4286790	33.72	22.6	27/08/2014	-27.95	684	968
S3.35	479794	4286785	38.72	22.7	27/08/2014			
S3.36	479803	4286782	52.53	23.9	27/08/2014	-28.81	717	985
S3.37	479810	4286778	65.81	40.0	27/08/2014			
S3.38	479771	4286786	46.06	22.1	27/08/2014	-28.94	664	973
S3.39	479782	4286783	49.94	22.0	27/08/2014			

S3.40	479790	4286780	20.62	20.6	27/08/2014	-27.88	660	1005
S3.41	479798	4286773	38.98	22.5	27/08/2014			
S3.42	479761	4286778	43.28	22.3	27/08/2014			
S3.43	479771	4286775	44.68	21.9	27/08/2014	-28.72	692	990
S3.44	479782	4286773	52.15	21.1	27/08/2014			
S3.45	479793	4286767	54.17	22.4	27/08/2014	-27.73	699	1005
S3.46	479800	4286759	109.02	37.5	27/08/2014			
S3.47	479765	4286767	38.77	20.6	27/08/2014	-27.31	697	1041
S3.48	479776	4286762	31.93	22.2	27/08/2014			
S3.49	479784	4286757	34.02	22.9	27/08/2014	-27.96	701	984
S3.50	479793	4286751	50.17	29.1	27/08/2014			
S3.51	479803	4286744	45.21	37.3	27/08/2014	-12.17	779	948
S3.52	479797	4286738	53.81	25.8	27/08/2014			
S3.53	479788	4286741	48.58	23.5	27/08/2014			
S3.54	479769	4286751	22.55	20.1	27/08/2014			
S3.55	479759	4286755	29.05	21.6	27/08/2014			
S3.56	479751	4286759	47.68	21.6	27/08/2014			
S3.57	479953	4286573	36.36	25.8	28/08/2014			
S3.58	479948	4286565	29.15	23.3	28/08/2014			
S3.59	479944	4286557	31.70	23.3	28/08/2014	-27.54	728	985
S3.60	479931	4286542	24.55	21.5	28/08/2014			
S3.61	479938	4286549	39.01	22.6	28/08/2014			
S3.62	479924	4286545	27.33	20.9	28/08/2014			
S3.63	479931	4286554	49.38	26.4	28/08/2014	-28.98	709	992
S3.64	479936	4286563	52.03	23.9	28/08/2014			
S3.65	479940	4286572	35.47	26.2	28/08/2014			
S3.66	479947	4286579	74.81	37.4	28/08/2014	-12.91	799	1078
S3.67	479938	4286584	182.10	50.0	28/08/2014			
S3.68	479933	4286575	92.86	45.9	28/08/2014	-7.69	932	1191

S3.69	479928	4286567	116.67	47.0	28/08/2014	-6.54	1180	1706
S3.70	479908	4286545	13.85	19.7	28/08/2014			
S3.71	479915	4286552	27.48	21.0	28/08/2014			
S3.72	479920	4286560	27.21	24.0	28/08/2014			
S3.73	479928	4286579	40.24	27.4	28/08/2014			
S3.74	479910	4286552	5.04	20.5	28/08/2014			
S3.75	479900	4286545	42.13	20.3	28/08/2014	-30.41	693	981
S3.76	479916	4286561	21.45	21.3	28/08/2014			
S3.77	479922	4286571	47.69	22.2	28/08/2014			
S3.78	479937	4286591	23.45	37.2	28/08/2014	-15.40	741	1009
S3.79	479923	4286595	32.28	22.3	28/08/2014			
S3.80	479926	4286591	665.04	47.6	28/08/2014	-4.70	4009	5054
S3.81	479924	4286604	249.11	44.3	28/08/2014			
S3.82	479932	4286612	30.13	22.7	28/08/2014			
S3.83	479935	4286622	16.29	21.8	28/08/2014	-27.29	734	909
S3.84	479941	4286631	32.48	20.0	28/08/2014			
S3.85	479945	4286638	21.20	20.7	28/08/2014			
S3.86	479953	4286648	617.38	59.1	28/08/2014	-4.06	1874	2701
S3.87	479810	4286808	61.02		26/08/2014			
S3.88	479810	4286809	228.46	54.2	26/08/2014			
S3.89	479830	4286798	1353.06	95.2	26/08/2014			
S3.90	479830	4286793	23.66	28.7	26/08/2014			
S3.91	479827	4286799	19.91	26.1	26/08/2014			
S3.92	479818	4286812	8.09	27.1	26/08/2014			
S3.93	479801	4286818	75.72	52.4	26/08/2014			
S3.94	479790	4286847	11.02	22.6	26/08/2014			
S3.95	479803	4286854	61.83	23.3	26/08/2014			
S3.96	479806	4286862	28.89	19.9	26/08/2014			
S3.97	479815	4286853	30.70	23.6	26/08/2014			

S3.98	479823	4286849	17.37	20.4	26/08/2014			
S3.99	479811	4286832	29.83	28.1	26/08/2014			
S3.100	479819	4286828	858.04	62.2	26/08/2014			
S3.101	479830	4286818	1068.50	70.9	26/08/2014			
S3.102	479857	4286793	106.12	88.3	26/08/2014			
S3.103	479857	4286797	11.02	31.8	27/08/2014			
S3.104	479872	4286810	204.17	51.3	27/08/2014	-5.06	915	4138
S3.105	479871	4286814	36.68	28.0	27/08/2014			
S3.106	479863	4286828	15.57	19.7	27/08/2014	-25.45	560	825
S3.107	479884	4286844	21.61	33.6	27/08/2014	-23.39	578	998
S3.108	479869	4286806	26.59	20.8	27/08/2014			
S3.109	479872	4286807	450.19	47.6	27/08/2014	-4.80	907	2117
S3.110	479872	4286807	42.96	23.2	27/08/2014			
S3.111	479882	4286813	42.22	21.8	27/08/2014	-29.78	603	882
S3.112	479887	4286807	12.33	21.8	27/08/2014			
S3.113	479874	4286795	37.98	42.7	27/08/2014			
S3.114	479873	4286804	71.11	24.7	27/08/2014	-27.76	618	983
S3.115	479893	4286815	18.87	21.6	27/08/2014			
S3.116	479893	4286814	20.80	20.6	27/08/2014	-27.75	605	824
S3.117	479877	4286785	41.91	21.5	27/08/2014	-27.79	582	1053
S3.118	479881	4286787	19.24	21.2	27/08/2014			
S3.119	479892	4286794	26.96	21.8	27/08/2014	-28.62	643	907
S3.120	479885	4286775	19.43	22.1	27/08/2014			
S3.121	479885	4286775	114.70	22.1	27/08/2014			
S3.122	479892	4286779	61.89	21.8	27/08/2014	-27.42	652	949
S3.123	479914	4286781	38.05	21.8	27/08/2014			
S3.124	479914	4286781	58.10	23.4	27/08/2014	-28.03	670	1101
S3.125	479900	4286770	59.40	22.6	27/08/2014			
S3.126	479895	4286766	65.94	22.0	27/08/2014	-28.17	635	902

S3.127	479869	4286797	46.45	22.2	27/08/2014			
S3.128	479858	4286785	260.84	72.0	27/08/2014			
S3.129	479855	4286782	45.21	35.6	27/08/2014	-14.07	566	865
S3.130	479837	4286775	40.35	44.7	27/08/2014			
S3.131	479836	4286771	119.18	54.7	27/08/2014	-6.05	580	917
S3.132	479824	4286760	27.52	27.9	27/08/2014			
S3.133	479820	4286753	67.56	27.6	27/08/2014	-26.05	615	962
S3.134	479812	4286746	30.32	28.1	27/08/2014			
S3.135	479808	4286738	47.95	24.9	27/08/2014	-26.23	677	911
S3.136	479801	4286730	49.32	24.9	27/08/2014			
S3.137	479807	4286727	39.73	23.6	27/08/2014	-27.92	647	977
S3.138	479816	4286735	54.86	28.8	27/08/2014			
S3.139	479819	4286744	40.78	26.6	27/08/2014	-27.88	606	882
S3.140	479836	4286753	454.67	82.1	27/08/2014			
S3.141	479836	4286754	168.87	48.8	27/08/2014	-7.45	620	840
S3.142	479841	4286770	156.54	58.6	27/08/2014			
S3.143	479848	4286770	80.95	28.6	27/08/2014	-9.01	572	902
S3.144	479859	4286788	37.42	30.4	27/08/2014			
S3.145	479861	4286788	174.78	49.5	27/08/2014	-6.00	675	1135
S3.146	479864	4286778	28.14	26.6	27/08/2014			
S3.147	479861	4286768	47.14	24.6	27/08/2014	-29.40	576	913
S3.148	479852	4286763	39.10	20.7	27/08/2014			
S3.149	479846	4286750	61.46	21.4	27/08/2014	-27.00	650	949
S3.150	479837	4286745	55.79	30.1	27/08/2014			
S3.151	479825	4286730	78.15	30.4	27/08/2014	-24.33	677	915
S3.152	479824	4286730	77.90	25.3	27/08/2014			
S3.153	479817	4286719	42.47	22.7	27/08/2014			
S3.154	479807	4286706	52.30	23.9	27/08/2014			
S3.155	479823	4286708	59.15	24.8	27/08/2014	-28.15	749	900

S3.156	479849	4286738	56.10	22.3	27/08/2014			
S3.157	479849	4286738	76.15	22.6	27/08/2014	-29.04	709	903
S3.158	479849	4286738	39.04	22.1	27/08/2014			
S3.159	479855	4286743	74.60	21.8	27/08/2014	-27.85	650	1041
S3.160	479856	4286743	46.70	21.5	27/08/2014			
S3.161	479877	4286755	51.06	21.0	27/08/2014			
S3.162	479877	4286755	61.02	20.7	27/08/2014			
S3.163	479871	4286750	33.00	22.2	27/08/2014	-27.95	614	908
S3.164	479872	4286750	50.50	20.5	27/08/2014			
S3.165	479864	4286742	37.67	20.7	27/08/2014			
S3.166	479858	4286735	59.90	20.8	27/08/2014			
S3.167	479851	4286731	78.77	21.5	27/08/2014	-26.36	637	919
S3.168	479845	4286723	56.73	21.4	27/08/2014			
S3.169	479838	4286712	47.76	20.9	27/08/2014			
S3.170	479835	4286702	51.99	22.0	27/08/2014			
S3.171	479822	4286687	64.20	22.0	27/08/2014			
S3.172	479825	4286675	38.61		27/08/2014			
S3.173	479811	4286753	125.16	36.7	27/08/2014	-6.71	636	1128
S3.174	479815	4286763	47.82	45.2	27/08/2014			
S3.175	479830	4286776	112.77	27.8	27/08/2014			
S3.176	479829	4286776	141.53	34.2	27/08/2014	-9.88	659	952
S3.177	479835	4286784	48.82	64.3	27/08/2014			
S3.178	479845	4286787	45.45	34.7	27/08/2014	-9.87	559	845
S3.179	479841	4286858	29.64	22.2	27/08/2014			
S3.180	479846	4286855	24.97	21.4	27/08/2014			
S3.181	479860	4286853	14.38	20.6	27/08/2014			
S3.182	479868	4286856	28.64	20.5	27/08/2014			
S3.183	479891	4286851	10.52	19.4	27/08/2014			
S3.184	479959	4286584	79.20	35.7	28/08/2014	-19.98	593	955

S3.185	479964	4286590	85.24	24.8	28/08/2014			
S3.186	479962	4286600	59.09	35.8	28/08/2014			
S3.187	479974	4286606	33.00	25.1	28/08/2014	-29.43	590	797
S3.188	479977	4286613	18.62	22.6	28/08/2014			
S3.189	479978	4286626	59.78	21.6	28/08/2014			
S3.190	479982	4286641	50.37	20.8	28/08/2014	-27.87	616	886
S3.191	479981	4286631	62.89	21.3	28/08/2014			
S3.192	479981	4286629	18.49	22.7	28/08/2014			
S3.193	479970	4286617	65.69	27.6	28/08/2014			
S3.194	479967	4286606	42.90	44.5	28/08/2014	-12.11	595	886
S3.195	479953	4286602	22.54	45.4	28/08/2014			
S3.196	479942	4286588	33.75	41.3	28/08/2014			
S3.197	479949	4286601	132.01	67.9	28/08/2014	-7.79	728	1276
S3.198	479949	4286601	306.29	71.0	28/08/2014			
S3.199	479952	4286611	54.05	55.6	28/08/2014			
S3.200	479954	4286618	294.83	57.3	28/08/2014	-6.45	797	1574
S3.201	479959	4286619	29.95	31.9	28/08/2014			
S3.202	479968	4286634	48.01	20.7	28/08/2014			
S3.203	479975	4286646	36.86	21.3	28/08/2014	-28.74	565	860
S3.204	479967	4286644	20.49	19.5	28/08/2014			
S3.205	479953	4286631	16.50	20.5	28/08/2014			
S3.206	479957	4286623	34.18	28.0	28/08/2014			
S3.207	479955	4286606	33.94	50.6	28/08/2014			
S3.208	479947	4286609	74.28	51.6	28/08/2014	-6.50	665	919
S3.209	479940	4286604	541.47	73.3	28/08/2014	-5.61	1045	2296
S3.210	479926	4286608	53.49	52.7	28/08/2014			
S3.211	479925	4286608	36.55	22.4	28/08/2014			
S3.212	479938	4286613	32.13	37.5	28/08/2014			
S3.213	479940	4286629	35.24	34.3	28/08/2014	-26.12	598	944

S3.214	479950	4286631	43.03	38.1	28/08/2014			
S3.215	479952	4286638	13.33	21.6	28/08/2014			
S3.216	479959	4286639	14.26	20.5	28/08/2014	-29.13	562	786
S3.217	479964	4286659	12.58	21.0	28/08/2014			
S3.218	479954	4286654	167.19	41.9	28/08/2014			
S3.219	479943	4286660	15.63	23.2	28/08/2014			
S3.220	479940	4286658	16.25	21.6	28/08/2014			
S3.221	479940	4286651	29.08	21.9	28/08/2014			
S3.222	479932	4286644	17.00	20.7	28/08/2014			
S3.223	479921	4286625	8.28	20.7	28/08/2014			
S3.224	479921	4286625	21.92	21.1	28/08/2014	-27.50	543	803
S3.225	479918	4286618	34.36	24.1	28/08/2014			
S3.226	479914	4286609	34.75	26.1	28/08/2014			
S3.227	479910	4286599	101.88	29.2	28/08/2014	-9.71	981	1281
S3.228	479906	4286591	19.24	21.6	28/08/2014			
S3.229	479903	4286582	20.63	19.8	28/08/2014			
S3.230	479899	4286573	25.40	19.2	28/08/2014			
S3.231	479928	4286626	7.17	22.8	28/08/2014			
S3.232	479924	4286616	23.37	22.8	28/08/2014			
S3.233	479934	4286633	19.39	19.8	28/08/2014			
S3.234	479938	4286643	17.69	21.3	28/08/2014			
S3.235	479942	4286651	441.81	43.5	28/08/2014	-6.36	1669	2178
S3.236	479936	4286537	49.69	22.6	28/08/2014			
S3.237	479944	4286544	49.32	22.1	28/08/2014			
S3.238	479947	4286553	52.30	23.0	28/08/2014			
S3.239	479950	4286561	50.37	23.3	28/08/2014	-27.33	591	896
S3.240	479957	4286573	49.44	24.7	28/08/2014			
S3.241	479962	4286582	70.61	28.8	28/08/2014	-26.89	812	1065
S3.242	479962	4286587	33.19	25.0	28/08/2014			

S3.243	479967	4286594	50.31	24.5	28/08/2014			
S3.244	479971	4286597	51.87	23.9	28/08/2014			
S3.245	479982	4286611	49.81	21.9	28/08/2014			
S3.246	479986	4286619	34.74	22.9	28/08/2014			
S3.247	479994	4286635	27.15	21.2	28/08/2014			
S3.248	479995	4286642	21.92	22.3	28/08/2014			
S3.249	479998	4286613	51.68	21.3	28/08/2014			
S3.250	479990	4286605	76.59	22.9	28/08/2014			
S3.251	479987	4286597	51.06	22.0	28/08/2014			
S3.252	479985	4286589	72.54	21.8	28/08/2014			
S3.253	479978	4286579	80.76	22.4	28/08/2014	-28.28	567	892
S3.254	479976	4286573	19.93	22.3	28/08/2014			
S3.255	479971	4286562	78.08	22.6	28/08/2014			
S3.256	479962	4286550	16.63	21.8	28/08/2014			
S3.257	479955	4286542	7.47	21.4	28/08/2014			
S3.258	479947	4286531	34.74	22.1	28/08/2014			
S3.259	479942	4286522	36.36	22.1	28/08/2014			
S3.260	479804	4286834	106.95	23.1	29/08/2014	-29.38	682	977
S3.261	479813	4286832	114.26	34.6	29/08/2014	-6.84	980	1281
S3.262	479824	4286825	269.36	47.0	29/08/2014	-6.45	1156	1669
S3.263	479835	4286818	73.40	60.0	29/08/2014	-6.95	839	1241
S3.264	479839	4286813	1043.54	93.8	29/08/2014	-7.29	6835	8083
S3.265	479852	4286807	854.58	85.9	29/08/2014	-5.59	3737	4813
S3.266	479860	4286800	369.40	82.7	29/08/2014	-4.97	3595	4659
S3.267	479865	4286795	21899.65	95.7	29/08/2014			
S3.268	479797	4286825	283.74	25.1	29/08/2014	-7.28	1525	2308
S3.269	479796	4286812	49.12	40.9	29/08/2014			
S3.270	479801	4286809	33.11	42.1	29/08/2014			
S3.271	479809	4286806	6.52	52.6	29/08/2014			

S3.272	479829	4286793	23.82	35.3	29/08/2014	-29.12	662	853
S3.273	479823	4286803	654.45	78.1	29/08/2014	-6.30	3180	3760
S3.274	479784	4286808	54.40	32.2	29/08/2014			
S3.275	479800	4286805	32.75	46.8	29/08/2014			
S3.276	479803	4286800	112.36	26.5	29/08/2014			
S3.277	479806	4286800	25.76	23.6	29/08/2014			
S3.278	479903	4286553	25.34	21.5	29/08/2014	-27.09	677	781
S3.279	479909	4286558	50.59	20.9	29/08/2014			
S3.280	479908	4286549	22.86	20.8	29/08/2014			
S3.281	479914	4286553	31.45	22.2	29/08/2014			

Table A.2 – Data recorded by the permanent station GTER1 during the surveys

Data	Barometric pressure (hPa)	Soil CO_2 flux (g m^{-2} d^{-1})	Soil temperature (ºC)	Soil water content (%)
01/07/2013 14:00	962	212	33.4	23.4
01/07/2013 15:00	962	218	33.4	23.2
01/07/2013 16:00	961	241	33.4	23.2
01/07/2013 17:00	961	241	33.4	23.2
01/07/2013 18:00	961	235	33.4	23.2
01/07/2013 19:00	961	222	33.4	23.0
02/07/2013 08:00				
02/07/2013 09:00				
02/07/2013 10:00				
02/07/2013 11:00	961	203	33.5	23.0
02/07/2013 12:00				
02/07/2013 13:00				
02/07/2013 14:00	960	165	33.6	22.8
02/07/2013 15:00	960	177	33.6	22.8
02/07/2013 16:00	960	179	33.6	22.8
02/07/2013 17:00	960	180	33.6	22.8
02/07/2013 18:00	959	171	33.6	22.8
02/07/2013 19:00	959	192	33.6	22.6
26/08/2013 09:00	958	257	37.9	21.7
26/08/2013 10:00	959	226	37.9	21.7
26/08/2013 11:00	959	267	37.9	21.7
26/08/2013 12:00				
26/08/2013 13:00				
26/08/2013 14:00	959	222	37.9	21.7

26/08/2013 15:00	958	221	37.9	21.9
26/08/2013 16:00	958	241	37.9	21.9
26/08/2013 17:00	958	230	37.9	21.9
27/08/2013 08:00	958	222	37.9	21.9
27/08/2013 09:00	959	204	37.9	21.9
27/08/2013 10:00	959	227	37.8	21.9
27/08/2013 11:00	959	218	37.9	21.9
27/08/2013 12:00	959	257	37.9	21.7
27/08/2013 13:00	959	242	37.9	21.9
27/08/2013 14:00	959	226	37.9	21.9
27/08/2013 15:00	959	228	37.9	21.9
27/08/2013 16:00	959	232	37.9	21.7
27/08/2013 17:00	959	218	37.9	21.7
27/08/2013 18:00	959	194	37.9	21.7
27/08/2013 19:00	959	244	37.9	21.7
30/05/2014 12:00	913	157	33.9	24.3
30/05/2014 13:00	913	108	33.9	24.1
30/05/2014 14:00	914	126	33.9	24.1
30/05/2014 15:00	905	104	33.9	24.1
30/05/2014 16:00	873	102	33.9	24.1
30/05/2014 17:00	862	103	33.9	24.1
30/05/2014 18:00	866	114	34.0	24.1
30/05/2014 19:00	867	121	34.0	24.1
31/05/2014 09:00	930	138	34.3	23.9
31/05/2014 10:00	894		34.3	23.9
31/05/2014 11:00	926		34.3	23.9
31/05/2014 12:00	939	118	34.3	23.9
31/05/2014 13:00	929	102	34.2	23.9

31/05/2014 14:00	871	108	34.2	23.9
31/05/2014 15:00	885	86	34.3	23.7
31/05/2014 16:00	874	86	34.3	23.9
31/05/2014 17:00	873	95	34.3	23.7
31/05/2014 18:00	870	97	34.3	23.9
31/05/2014 19:00	860	96	34.3	23.9
26/08/2014 08:00	849	173	37.8	25.6
26/08/2014 09:00	849	194	37.8	25.8
26/08/2014 10:00	850	221	37.8	25.6
26/08/2014 11:00	837	191	37.9	25.6
26/08/2014 12:00	844	222	37.9	26.0
26/08/2014 13:00	843	144	37.9	26.2
26/08/2014 14:00	840	161	37.9	26.4
26/08/2014 15:00	857	215	37.9	26.4
26/08/2014 16:00	922	179	38.0	26.4
26/08/2014 17:00	831	217	38.0	26.4
26/08/2014 18:00	838	227	38.0	26.4
26/08/2014 19:00	950	234	38.0	26.4
27/08/2014 08:00	828	214	38.1	26.2
27/08/2014 09:00	828	214	38.1	26.2
27/08/2014 10:00	837	190	38.1	26.2
27/08/2014 11:00	836		38.1	26.0
27/08/2014 12:00	846		38.1	26.0
27/08/2014 13:00	819		38.1	26.0
27/08/2014 14:00	841		38.1	26.2
27/08/2014 15:00	858		38.1	26.0
27/08/2014 16:00	878		38.1	26.0
27/08/2014 17:00	882	215	38.1	26.0

27/08/2014 18:00	871	223	38.1	26.0
27/08/2014 19:00	848	208	38.1	26.0
28/08/2014 08:00	847	193	38.1	25.8
28/08/2014 09:00	832	199	38.1	25.8
28/08/2014 10:00	829	205	38.1	25.8
28/08/2014 11:00	836	188	38.1	26.0
28/08/2014 12:00	837	223	38.1	25.8
28/08/2014 13:00	832		38.1	25.8
28/08/2014 14:00	834	173	38.1	25.8
28/08/2014 15:00	821	174	38.1	25.8
28/08/2014 16:00	840	223	38.1	25.8
28/08/2014 17:00	841	196	38.2	25.6
28/08/2014 18:00	839	215	38.2	25.6
28/08/2014 19:00	827	175	38.2	25.6
29/08/2014 08:00	850	258	38.1	26.2
29/08/2014 09:00	846	221	38.1	26.2
29/08/2014 10:00	855	183	38.1	26.4
29/08/2014 11:00	858		38.1	26.4
29/08/2014 12:00	844		38.1	26.4
29/08/2014 13:00	839		38.1	26.2
29/08/2014 14:00	835		38.1	26.2
29/08/2014 15:00	860		38.1	26.4
29/08/2014 16:00	865	213	38.1	26.2
29/08/2014 17:00	842	121	38.1	26.2
29/08/2014 18:00	840	181	38.1	26.2
29/08/2014 19:00	846	204	38.1	26.2
30/08/2014 08:00	868	129		26.2
30/08/2014 09:00	839	192		26.4

30/08/2014 10:00	835			26.2
30/08/2014 11:00	841		38.0	26.4
30/08/2014 12:00	845		38.0	26.2
30/08/2014 13:00	881		37.9	26.2
30/08/2014 14:00	828			26.2
30/08/2014 15:00	837			26.2
30/08/2014 16:00	842			26.2
30/08/2014 17:00	838		37.9	26.2
30/08/2014 18:00	836		37.9	26.2
30/08/2014 19:00	841		37.8	26.4

Appendix 3 – Variograms for the soil CO_2 fluxes measured on surveys 1 and 2 (respectively, on Summer 2013 and May 2014).

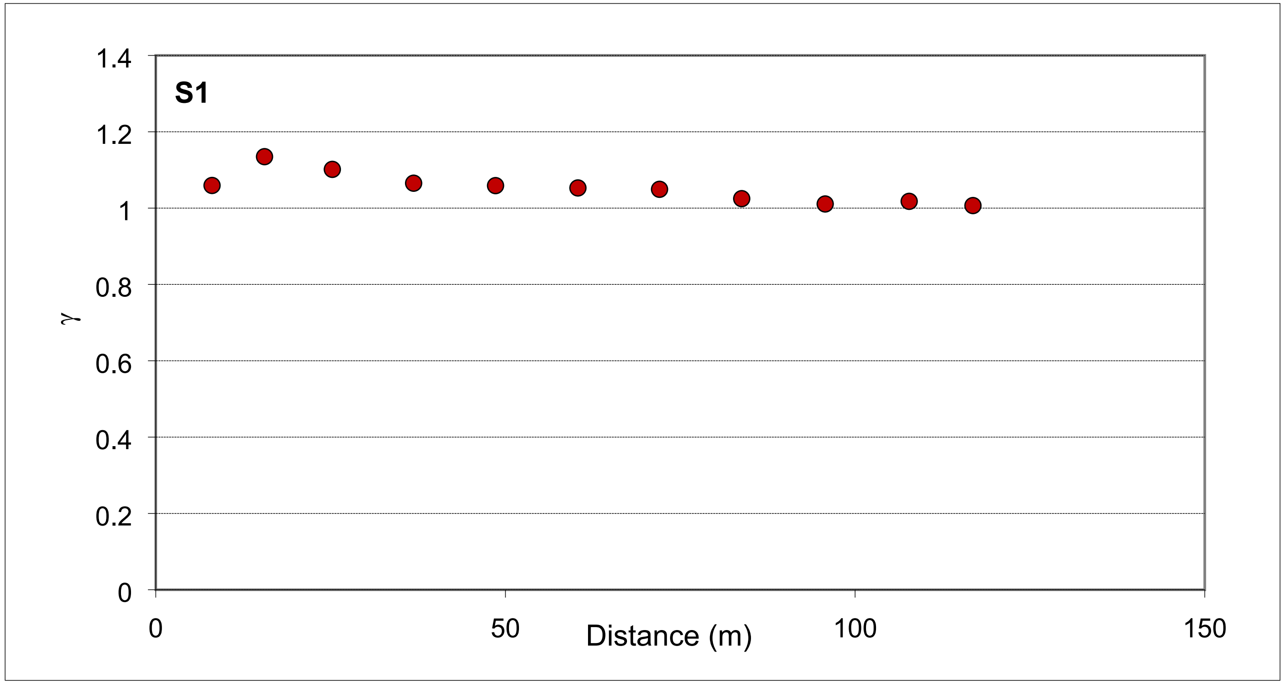

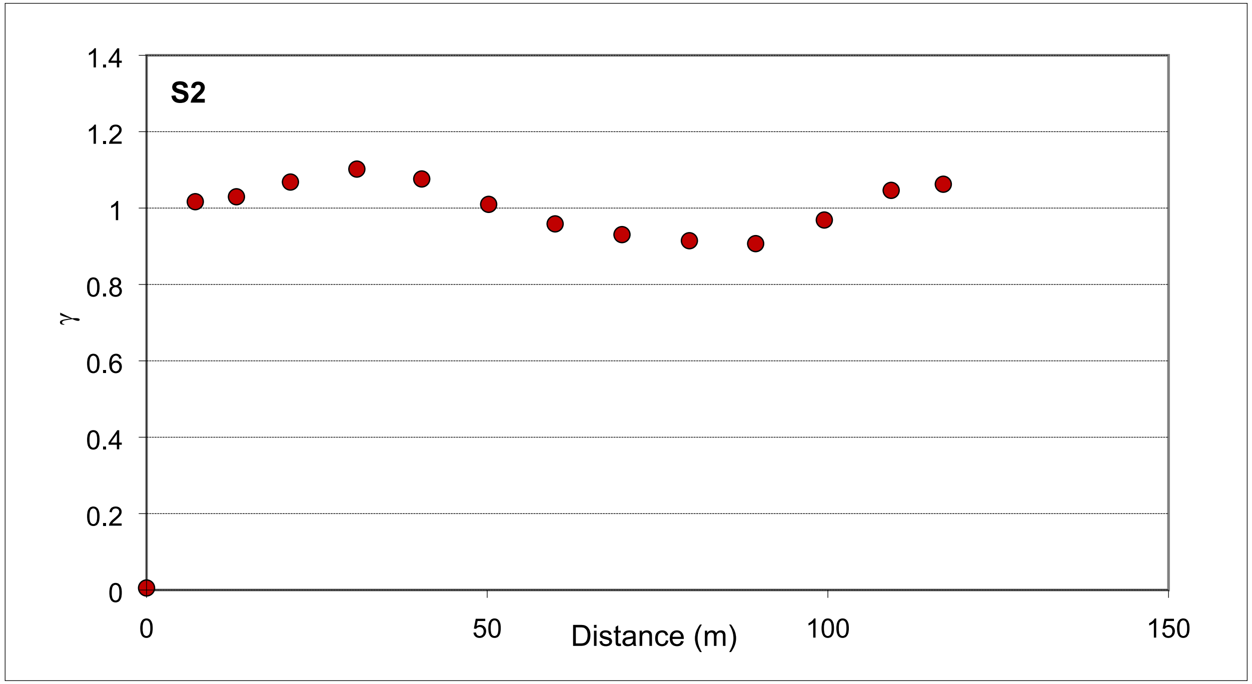

S2
1.4
1.2
1
0.8
0.6
0.4
0.2
0
γ
0
50
100
150
Distance (m)